**ONLINE MATERIAL**

# Age-associated Sirtuin 1 reduction in vascular smooth muscle links vascular senescence and inflammation to abdominal aortic aneurysm

Hou-Zao Chen[*,1], Fang Wang[*,1], Peng Gao[*,1], Jian-Fei Pei[*,1], Yue Liu[1], Ting-Ting Xu[1], Xiaoqiang Tang, Wen-Yan Fu[1], Jie Lu[1], Yun-Fei Yan[1], Xiao-Man Wang[1], Lei Han[1], Zhu-Qin Zhang[1], Ran Zhang[1], Ming-Hui Zou[2], De-Pei Liu[1]

[1]From the State Key Laboratory of Medical Molecular Biology, Department of Biochemistry and Molecular Biology， Institute of Basic Medical Sciences, Chinese Academy of Medical Sciences & Peking Union Medical College, Beijing 100005, China
[2]From the Division of Molecular Medicine, Department of Medicine, University of Oklahoma Health Sciences Center, Oklahoma City, Oklahoma, USA
*These authors contributed equally to this work.

Correspondence to De-Pei Liu, PhD, State Key Laboratory of Medical Molecular Biology, Department of Biochemistry and Molecular Biology, Institute of Basic Medical Sciences, Chinese Academy of Medical Sciences and Peking Union Medical College, No.5 Dong Dan San Tiao, Beijing 100005, P.R. China. Email address: liudp@pumc.edu.cn or
To Ming-Hui Zou, MD, PhD., the Center for Molecular and Translational Medicine, Georgia State University, Atlanta, GA 30303, USA. Email address: mzou@gsu.edu

## Online methods

### Animal experiments

All animal protocols were approved by the Animal Care and Use Committee at the Institute of Basic Medical Sciences, Chinese Academy of Medical Sciences and Peking Union Medical College.

We used 2- to 3-month-old C57BL/6J male mice as young mice and 18- to 20-month-old C57BL/6J male mice as aged mice. We established SV-Tg mice as previously described[1]. *Apoe*$^{-/-}$ mice in the C57BL/6J background were obtained from Peking University (Beijing, China). SIRT1-VSMC-specific transgenic (SV-Tg) *Apoe*$^{-/-}$ mice were generated by crossing SV-Tg mice with *Apoe*$^{-/-}$ mice. The F1 generation was backcrossed with *Apoe*$^{-/-}$ mice to produce the *Apoe*$^{-/-}$ genotype. *Apoe*$^{-/-}$ mice served as controls.

We utilized a Cre/LoxP strategy to yield SIRT1-VSMC-specific knockout (SV-KO) mice (Online Figure Ⅱ). *Sirt1*$^{flox/flox}$ mice in the 129 background were purchased from the Jackson Laboratory (Bar Harbor, Maine; Stock Number: 008041). A LoxP-flanked neomycin cassette immediately upstream of exon 4 and a third LoxP site downstream of exon 4 were inserted to create the targeted mutant Sirt1 allele. *Sirt1*$^{flox/flox}$ mice in the 129 background were backcrossed with mice in the C57BL/6J background for at least 10 generations to yield *Sirt1*$^{flox/flox}$ mice in the C57BL/6J background. *SM22α-Cre*$^{+/+}$ mice in the 129 background were purchased from the Jackson Laboratory (Bar Harbor, Maine; Stock Number: 006878). These mice have a Cre-recombinase gene inserted into the endogenous transgelin (*SM22α*) locus. *SM22α-Cre*$^{+/+}$ mice in the 129 background were backcrossed with mice in the C57BL/6J background for at least 10 generations to yield *SM22α-Cre*$^{+/+}$ mice in the C57BL/6J background. *Sirt1*$^{flox/flox}$ mice were crossed with *SM22α-Cre*$^{+/+}$ mice, both in the C57BL/6J background, to generate SV-KO mice. The F1 generation (*SM22α-Cre*$^{+/-}$; *Sirt1*$^{flox/+}$) was backcrossed with *Sirt1*$^{flox/flox}$ mice to fix the *Sirt1*$^{flox/flox}$ genotype. When *SM22α-Cre*$^{+/-}$; *Sirt1*$^{flox/flox}$ mice were obtained, they were backcrossed with *Sirt1*$^{flox/flox}$ mice to generate SV-KO (*SM22α-Cre*$^{+/-}$; *Sirt1*$^{floxflox}$) mice and WT (*Sirt1*$^{floxflox}$) littermates as controls.

*p21*$^{-/-}$ mice in the C57BL/6J background[2] were purchased from The Jackson Laboratory (stock number 016565). *p21*$^{-/-}$ *Apoe*$^{-/-}$ double knockout mice were generated by crossing *p21*$^{-/-}$ mice with *Apoe*$^{-/-}$ mice. The F1 generation was backcrossed with *Apoe*$^{-/-}$ mice to produce the F2 *p21*$^{+/-}$*Apoe*$^{-/-}$ genotype. Then *p21*$^{+/-}$*Apoe*$^{-/-}$ mice were mated with themselves to produce three genotypes of F3 generation including 1/4 ratio of *p21*$^{-/-}$*Apoe*$^{-/-}$ double knockout mice and 1/4 ratio of *Apoe*$^{-/-}$ mice. *Apoe*$^{-/-}$ mice were served as controls.

All mice were genotyped by PCR conducted on toe clip samples; primers are listed in Online Table Ⅷ.

### Analyses and quantification of Ang II-induced AAAs

We used 4- to 6-month-old male mice on a normal chow diet. All age-matched mice (*Apoe*$^{-/-}$, SV-Tg *Apoe*$^{-/-}$, *p21*$^{-/-}$ *Apoe*$^{-/-}$, SV-KO, and WT) were infused with Ang II (Sigma-Aldrich, St Louis, MO, USA, Cat. No. A9525) at a dosage of 1.44 mg·kg$^{-1}$·d$^{-1}$ or saline for 4 weeks using Alzet osmotic pumps (model

2004; DURECT Corp.). The detailed manipulation was performed as previously described[3]. In the last week of the experiment, the mice underwent all physiologic assessments and then were sacrificed. The direct method was used to measure the outer diameter of the suprarenal aorta. After the aorta was dissected free from the surrounding connective tissue, a ruler was set aside and a picture was taken with a digital camera. The image of the aorta was used to measure the outer diameter of the suprarenal aorta by a researcher blind to group assignment. Suprarenal regions of abdominal aorta were identified between the last pair of intercostal arteries and the right renal branch. The adventitial circumferences at the maximal expanded portion of the suprarenal aorta were quantified as the maximal abdominal aortic diameter. The maximum width of the abdominal aorta was analyzed using Image Pro Plus software (Media Cybernetics) after adjusting the scale according to the ruler in aorta pictures. At least 3 measurements of the maximal expanded portion of the suprarenal aorta for each mouse were averaged before calculating the mean of each experimental group. Aneurysm formation was defined as the increase in the external width of the suprarenal aorta by 50% or greater compared with that in saline-infused mice as previously described.[3]

**Analyses and quantification of $CaCl_2$-induced AAAs**

We also induced AAA in mice (WT, SV-Tg or SV-KO) by periaortic application of 0.5 mol/l $CaCl_2$ as previously described with little modification[4]. Briefly, mice aged 8-12 weeks were anesthetized and underwent laparotomy. The abdominal aorta between the renal arteries and bifurcation of the iliac arteries was dissociated from the surrounding retroperitoneal structures under a stereo microscope (Nikon). Then, 0.5 mol/l $CaCl_2$-treated cotton gauze was applied to the external surface of the aorta. NaCl (0.9%) was used in the sham control mice instead of $CaCl_2$. After 15 minutes the incision was closed after aorta was rinsed with saline and the mice were allowed to recover. Three (SV-KO) or six (SV-Tg) weeks later, the mice were sacrificed and underwent laparotomy. Infrarenal regions of abdominal aorta were identified between the right renal branch and bifurcation of the iliac arteries. The methods used for quantification of $CaCl_2$-induced AAAs are described in Methods section of Ang II-induced AAAs on infrarenal regions instead of suprarenal regions. The aortic internal diameter of mice was assessed in a blinded manner using a VisualSonics Vevo770 ultrasound biomicroscope (VisualSonics Inc, Toronto, ON, Canada) with a 30-MHz linear array ultrasound transducer and the inner lumen diameter at the maximal expanded portion of the infrarenal aorta were quantified as the internal maximal diameter.

**Blood pressure and serum lipid measurements**

The heart rate and systolic blood pressure of the animals were measured using tail-cuff plethysmography (BP-2000 System; Visitech Systems, Apex, NC) as described previously[1]. Blood samples were obtained from the mice before sacrifice. Serum cholesterol, triglyceride, high-density lipoprotein cholesterol (HDL-C), and low-density lipoprotein cholesterol (LDL-C) levels were measured at the clinical laboratory of Peking Union Medical College Hospital.

**Transit-time (TT) method for performing pulse-wave velocity (PWV) measurements**

The TT method estimates the PWV from the pressure wave transit time between two measurement locations separated by a known distance as previously described[5]. Pulse-wave Doppler ultrasound velocity measurements were consecutively performed at the distal and proximal locations while

simultaneously recording the electrocardiogram (ECG) signal over a short period, during which the mouse was observed to have stable heart and breathing rates. TT was determined by subtracting the distal arrival time between the ECG R-wave peak and the foot of the velocity upstroke from the similarly determined proximal arrival time. As a threshold for consistent detection of the upstroke, arrival times were calculated relative to the time at which 20% of the peak value was attained. The left common carotid artery (LCCA) was chosen as a measurement target because it was easily accessible and offered a uniform and branch-free pathway of over approximately 10 mm between the aortic arch and the bifurcation. The distance between measurement sites was determined from a B-mode image encompassing both the distal and proximal locations. Proximal velocity measurements were taken 1 mm downstream from the aortic arch. Distal velocity measurements were taken 1.5 mm upstream from the bifurcation.

TT measurements were performed using a VisualSonics Vevo770 ultrasound biomicroscope (VisualSonics Inc., Toronto, ON, Canada). The mechanically scanned, single-element transducer had a 6-mm focal length and an f-number of 2. B-mode data were acquired at 40 MHz with a 30 frame-per-second (fps) frame rate. Doppler data were acquired at 30 MHz with a 50 kHz pulse-repetition frequency (PRF). The ECG signal was detected using a heart rate monitoring system (VisualSonics Inc., Toronto, ON, Canada) smoothed with a 1-kHz low-pass filter and digitized by the Vevo770 system at 8 kHz. The results were processed using VisualSonics analysis software.

**SIRT1 deacetylase activity assay**

SIRT1 activity was assayed using a SIRT1 deacetylase activity assay kit (Sigma) according to the manufacturer's instructions. Briefly, SIRT1 was immunoprecipitated using a SIRT1 antibody (Millipore) from whole-aorta homogenates (200 μg of protein) in immunoprecipitation (IP) buffer. The SIRT1 substrate reagent and $NAD^+$ were added to the SIRT1-conjugated beads (sc-2002; Santa Cruz Biotechnology) and incubated at 37 °C for 80 minutes after final washing. The substrate-SIRT1 mixture was placed on a 96-well plate, and the developer reagent was added to the wells at 37 °C for 20 minutes. The plate was read using a spectrophotometer with an excitation wavelength of 360 nm and an emission wavelength of 445 nm (Synergy 4 microplate reader; BioTek).

**SA-β-gal activity assay**

SA-β-gal activity was quantitatively measured according to the rate of conversion of 4-methylumbelliferyl-β-d-galactopyranoside (MUG) to the fluorescent hydrolysis product 4-methylumbelliferone (4-MU) at pH 6.0, as described previously[6]. Briefly, aorta tissues were homogenized in the lysis buffer (5 mM CHAPS, 40 mM citric acid, 40 mM sodium phosphate, 0.5 mM benzamidine, and 0.25 mM PMSF, pH 6.0) and kept on ice for 1 h. The lysates were centrifuged at 12,000 × *g* for 5 mins, and the supernatant was mixed with 2× reaction buffer (40 mM citric acid, 40 mM sodium phosphate, 300 mM NaCl, 10 mM β-mercaptoethanol, and 4 mM $MgCl_2$ [pH 6.0] with 1.7 mM MUG), which was placed into a 37 °C water bath for 3 h. We added 50 μL reaction mix to 500 μL 400 mM sodium carbonate stop solution (pH 11.0), which was read at 150 μL/well in a 96-well plate using a Synergy 4 plate reader (BioTek) with excitation at 360 nm and emission at 465 nm. Normalized SA-β-gal activity was expressed as the observed fluorescence divided by the mg of total protein in the assay.

The whole-aorta tissues were stained to determine SA-β-gal activity using a commercial kit (ab65351; Abcam) according to the manufacturer's instructions, as previously reported[7]. Briefly, the aortas were fixed in 2% formaldehyde containing 0.2% glutaraldehyde for 15 minutes and washed with PBS twice; subsequently, samples were incubated at 37 °C for 24 h in the staining solution (1 mg/ml X-gal in dimethylformamide, 5 nM potassium ferrocyanide, 5 nM potassium ferricyanide, 40 mM citric acid/sodium phosphate, 0.15 M NaCl, and 2 mM $MgCl_2$, pH 5.9). The cells with blue color were considered SA-β-gal positive. In primary vascular smooth muscle cells (VSMCs), SA-b-gal activity was also determined as previously described.[8] VSMCs were counterstained with 2.5 μg $mL^{-1}$ DAPI, and the proportion of SA-b-gal activity-positive cells was quantified using light and fluorescence microscopy.

**Histological analyses**

After hemodynamic measurements, the animals were sacrificed. After the mice were sacrificed, aortas from the ascending aorta to the bifurcation of the common iliac artery were isolated. After macroscopic analysis, suprarenal abdominal aortas were subjected to histology analysis. For morphological analysis, the aortas were perfused with normal saline and fixed with 4% paraformaldehyde-PBS at physiological pressure for 5 minutes. Whole aortas were harvested, fixed for 24 h, and embedded in paraffin. For characterization of cross sections, aortic sections were collected serially from the proximal to the distal aorta. Histology was determined in sections (5 μm each) that were taken from suprarenal regions of abdominal aorta at intervals of 500 μm. At least 10 sections were analyzed per mouse. Paraffin sections were stained with elastin van Gieson staining or used for immunostaining. For the semi-quantification of elastin degradation, we used a standard for the elastin degradation score as previously described[3]. The grades were as follows: score 1, no degradation; score 2, mild elastin degradation; score 3, severe elastin degradation; score 4, aortic rupture. Elastic fiber content was quantified as described previously.[9] Briefly, after the cross sections were stained with elastin van Gieson staining, elastic fiber content was quantified in five separate representative images of each section by a single blinded observer using Image Pro Plus software (Media Cybernetics) after adjusting the scale. The areas of aortic media and the elastic fibers were calculated after they were individually outlined. The respective areas were averaged from all the images of a given aortic section and the ratio of elastic fiber content to total aortic media was determined.

**Immunohistochemistry**

Slides were deparaffinized, and endogenous peroxidase activity was quenched with 3% (vol./vol.) hydrogen peroxide in 10% PBS for 10 mins. Nonspecific binding sites were blocked with 10% bovine serum in PBS at room temperature for 1 h. The slides were incubated at 4 °C overnight with diluted primary antibodies and with biotinylated secondary antibody at 37 °C for 30 mins and subsequently with horseradish peroxidase-labeled streptavidin solution at 37 °C for 20 mins. The slides were then stained with diaminobenzidine and counterstained with hematoxylin. The primary antibodies used were human SIRT1 (1104-1, 1:250 dilution; EPITOMICS), α-smooth muscle actin (A5691, 1:400 dilution; Sigma-Aldrich), p21 (ab2961, 1:80 dilution; Abcam), MCP-1 (sc-1784, 1:400 dilution; Santa Cruz), leukocyte common antigen, CD45 (clone Ly-5, 1:100 dilution; BD Pharmingen), 8-OH-dG (MOG-020P, 1:100 dilution; Japan Institute for the Control of Aging), and nitrotyrosine (06-284, 1:500 dilution;

Millipore). The medial 8-OH-dG or nitrotyrosine content in the suprarenal aortic wall of mice was analyzed by calculating the integration optical density value of positive staining within the media using Image-Pro Plus software (Media Cybernetics). A mean value was determined from at least four sections in each animal.

**Immunofluorescent staining**

Suprarenal abdominal aortas from young and aged mice were subjected to immunofluorescent analysis. The aortas were fixed with 4% paraformaldehyde-PBS for 24 hours, embedded in paraffin, and serial sections (5 μm each) at 500 μm intervals were made using suprarenal abdominal aortas as previously described.[3] After slides were deparaffinized, nonspecific binding sites were blocked in 10% bovine serum in PBS at room temperature for 1 h. The slides were then incubated at 4 °C overnight with diluted primary antibodies and with fluorescent-coupled secondary antibodies at 37 °C for 45 mins in the dark followed by DAPI for 5 mins at room temperature in the dark. The slides were then rinsed with PBS and evaluated under a fluorescence microscope. The primary antibodies used were human SIRT1 (LS-B4520, 1:100 dilution; LifeSpan Biosciences), mouse SIRT1 (07-131, 1:100 dilution; Millipore), and α-smooth muscle actin (A5691, 1:100 dilution; Sigma-Aldrich).

**Cell culture, adenovirus generation and infection**

Primary VSMCs were isolated from 2- to 3-month-old male mice and maintained in Dulbecco's modified Eagle's medium (DMEM) containing 15% FBS at 37 °C in a humidified atmosphere of 5% $CO_2$ and 95% air as previously described[9]. Passages 3 to 6 of VSMCs at 70-80% confluence were used for experiments. Human aortic smooth muscle cells (HASMCs) were purchased from ScienCell (Cat No: 6110, ScienCell) and cultured in Smooth Muscle Cell Medium (SMCM, Cat No: 1101, ScienCell) supplemented with 100 U/ml penicillin, 100 μg/ml streptomycin, smooth muscle cell growth supplement (SMCGS, Cat. No. 1152, ScienCell), and 10% FBS. The adenovirus-mediated knockdown of SIRT1 (Ad-SIRT1 RNAi), p21 (Ad-p21 RNAi) and control vector (Ad-U6) were generated using the AdEasy vector kit (Quantum Biotechnologies) as described in the supplier's protocol. The RNAi sequences were reported previously[10, 11]. The VSMCs were infected for 24 hours with the above adenovirus at an MOI of 100, washed and incubated in 10% FBS-medium without virus and treated with saline, 100 nM angiotensin II (Sigma) or 10 mM $CaCl_2$ (Sigma) for 24 hours.

**Real-time PCR**

Total RNA was extracted using TRIzol reagent (Invitrogen) according to the manufacturer's protocol. Two micrograms of total RNA was used for the first-strand synthesis with cDNA M-MuLV Reverse Transcriptase (New England Biolabs) using random primers. The QuantiTect SYBR Green RT-PCR Kit (QIAGEN) was used for the amplification reactions using the 1-step protocol described by the manufacturer with the Applied Biosystems Real-time PCR Detection System. The fluorescence curves were analyzed using StepOne Software (Version 2.1). The primers are listed in Online Table VIII.

**Western blot analyses**

Western blots were performed as described previously[12]. The primary antibodies used were human SIRT1 (1104-1, 1:1000 dilution; EPITOMICS), human MCP-1 (ab9669, 1:1000 dilution; Abcam), human and mouse MMP2 (sc-13595, 1:1000 dilution; Santa Cruz), human and mouse GAPDH (5174, 1:3000 dilution; Cell Signaling Technology), β-actin (4970, 1:3000 dilution; Cell Signaling Technology), mouse SIRT1 (07-131, 1:1000 dilution; Millipore), mouse p53 (Sc-73566, 1:1000 dilution; Santa Cruz), mouse Ac-p53 (06-758, 1:500 dilution; Millipore), mouse p21 (05-345, 1:1000 dilution; Millipore), mouse MCP-1 (ab7202, 1:2000 dilution; Abcam), mouse MT1-MMP (ab51074, 1:2000 dilution; Abcam), mouse TIMP2 (ab1828, 1:2000 dilution; Abcam), mouse TIMP1 (sc-5538, 1:1500 dilution; Santa Cruz), mouse p65 (8242, 1:1000 dilution; Cell Signaling Technology), mouse Phospho-NF-κB p65 (Ser536) (3033, 1:1000 dilution; Cell Signaling Technology). Western blots were quantified densitometrically using Quantity One software (Bio-Rad), and the intensity values were normalized to GAPDH or β-actin.

**Matrix metalloproteinase (MMP) activity**

The detection of MMP activity was performed as previously reported[13]. Five micrograms of protein in aorta homogenates was electrophoresed in SDS-PAGE gels containing gelatin. The gels were washed with 2.5% Triton X-100 for 30 mins and incubated for 12-40 h in zymography development buffer at 37 °C. The gel was subsequently stained with Coomassie brilliant blue.

**Chromatin immunoprecipitation**

ChIP assays were carried out as previously described.[14] Briefly, cells or tiny tissue pieces were cross-linked with 1% formaldehyde at room temperature for 10 min. The reaction was quenched with 125 mM glycine. Cells were collected, washed twice with cold PBS and resuspended in cell collection buffer (100 mM Tris-HCl, pH 9.4, with 10 mM DTT and complete protease inhibitor cocktail (Sigma) at room temperature for 30 min and 30 °C for 15 min. Nucleus/Chromatin preparation buffers I and II (buffer I: 10 mM EDTA, 0.5 mM EGTA, 10 mM Hepes, pH 6.5, with 0.25% Triton X-100; buffer II:1 mM EDTA, 0.5 mM EGTA, 10 mM Hepes, pH 6.5, 200 mM NaCl; Both are freshly added with complete protease inhibitor cocktail (Sigma)) were used to isolate nuclei. The pellet of nuclei was washed with cold PBS and resuspended in SDS lysis buffer (10 mM EDTA, 50 mM Tris-HCl, pH 8.1, 0.5% Empigen BB (Sigma), 1% SDS and Complete Protease Inhibitor (Sigma)). Nuclear extracts were sonicated to generate chromatin fragment with an average size of 0.3 kb on a Bioruptor Plus sonication system (Diagenode). Chromatin lysate was cleared by centrifugation, diluted with 10 volumes of ChIP dilution buffer (16.7 mM Tris-HCl, pH 8.1, with 0.01% SDS, 1.1% Triton X-100, 1.2 mM EDTA, 167 mM NaCl and Complete Protease Inhibitor; precleared with Dynabead protein A (Invitrogen) and subjected to immunoprecipitation with ChIP-grade antibody against normal rabbit IgG (ab46540, Abcam)or RelA/p65 (ab7970, Abcam). DNA-protein complex was precipitated with Dynabead protein A (Invitrogen), eluted in washing buffers I-IV. (buffer I: 2 mM EDTA, 20 mM Tris-HCl, pH 8.1, 0.1% SDS, 1% Triton X-100, 150 mM NaCl; buffer II: 2 mM EDTA, 20 mM Tris-HCl, pH 8.1, 0.1% SDS, 1% Triton X-100, 500 mM NaCl; buffer III: 10 mM Tris-HCl, pH 8.1, 1 mM EDTA, 250 mM LiCl, 1% Deoxycholate (Sigma), 1% NP-40; buffer IV: 10 mM Tris-HCl, pH 8.1, 1 mM EDTA) and treated with Proteinase K and RNase A in turn to reverse cross-links. DNA was purified with the QIAquick PCR purification kit or the Mini-Elute PCR purification kit (Qiagen) and analyzed by quantitative RT-PCR (LightCycler 96, Roche) with primers that targeted interesting DNA sequences. We analyzed mouse or

human MCP-1 promoters using AliBaba2.1 (www.generegulation.com/pub/programs/alibaba2) to find the potential binding sites of interested transcription factors. Primer sequences were listed in Online Table Ⅸ.

**Statistical analyses**

For all statistical tests, a P value of <0.05 was considered statistically significant, and all tests were 2-tailed. Fisher's exact test was applied to the comparisons of AAA incidence and log-rank (Mantel-Cox) test was used for survival comparison between groups. Normality tests were assessed via the Shapiro-Wilk statistics with SPSS software package (version 19.0). Normally distributed datasets were analyzed with the unpaired Student's *t* test for 2 independent groups or paired *t* test for 2 dependent groups, and the one-way analysis of variance (ANOVA) followed by the post Bonferroni's multiple comparisons test for ⩾3 groups. Quantitative results are expressed as the mean ± standard deviation (SD) for normally distributed datasets. Where a normal distribution could not be confirmed, nonparametric tests were used (Mann-Whitney U test for 2 independent group, Wilcoxon signed rank test for 2 paired groups and the Kruskal-Wallis test with post Dunn's multiple comparisons test for ⩾3 groups) and quantitative results are expressed as the median with interquartile range. All statistical analyses were performed using GraphPad Prism (version 6.01) software and the detailed statistical methods were listed in Online Table Ⅹ.

**Online Figures and legends**

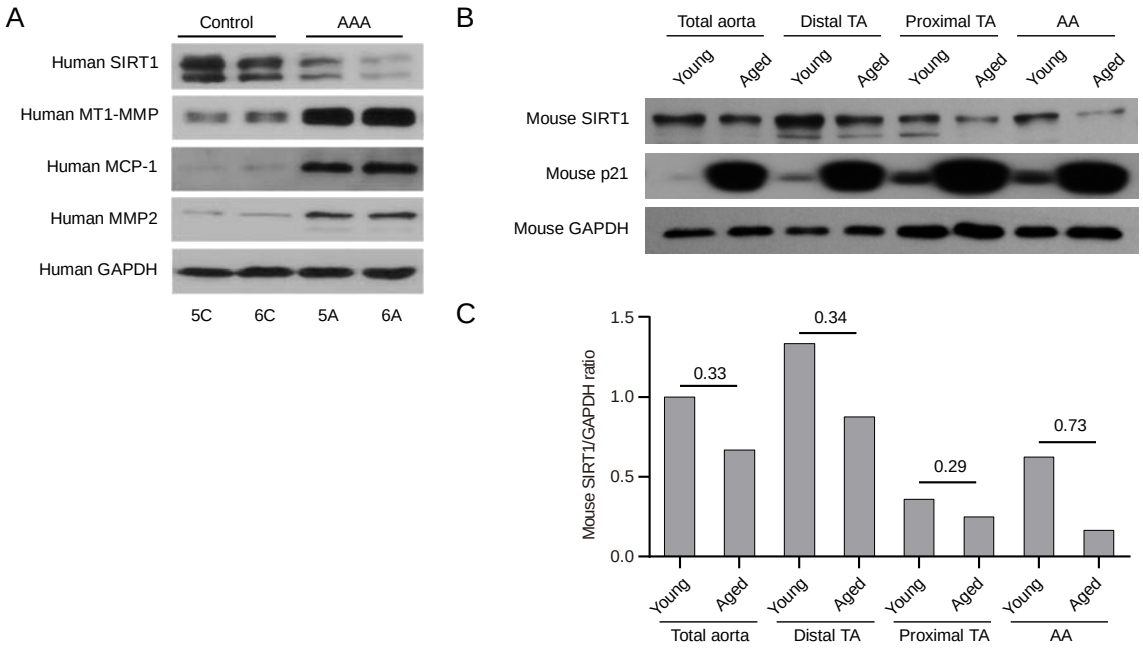


**Online Figure Ⅰ** SIRT1 expression in human AAAs and in aged mouse aortas. (**A**) The expression of SIRT1 and several VSMC-related molecules in human AAA samples (5, 6). (**B**) Western blots of SIRT1 and p21 proteins in the different sections of aorta homogenates from young and aged mice. (**C**) Densitometric analysis of the protein level of SIRT1 in the different regions of aortas from young and aged mice. The numbers on the top indicate the SIRT1 reduction in aged aorta compared with that in young aorta. The whole aorta is divided into three parts as follows: the proximal thoracic aorta (the ascending aorta and transverse aortic arch), the distal thoracic aorta (the descending thoracic aorta) and the abdominal aorta. Adventitial tissue was removed from the aorta as much as possible and each vascular section from five aortas was pooled together for immunoblot. TA, thoracic aorta. AA, abdominal aorta.

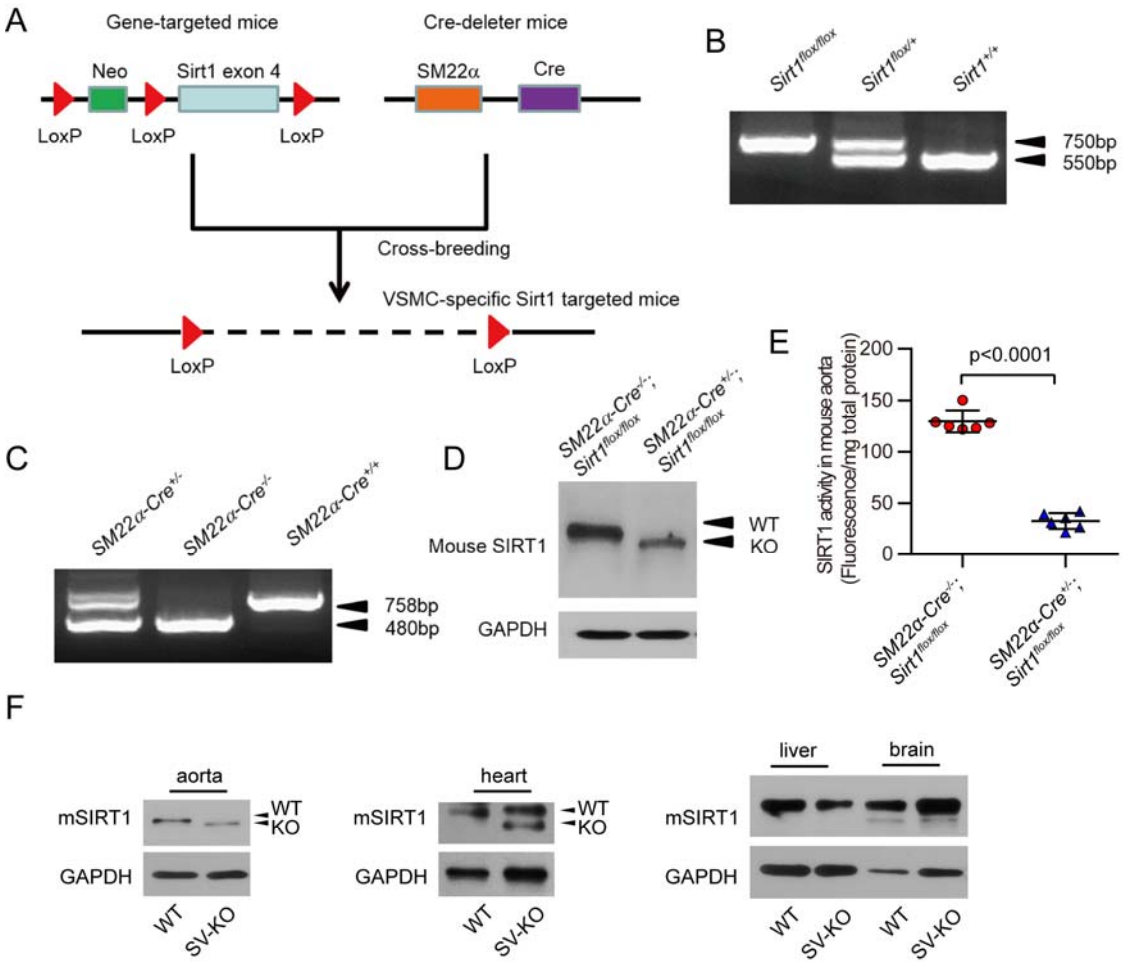


**Online Figure Ⅱ** Generation and assessment of a VSMC-specific *Sirt1* KO mouse model. (**A**) Strategy applied to delete *Sirt1* in mouse VSMCs. Sirt1 exon 4 is flanked by LoxP sites. (**B-C**) PCR genotyping on genomic DNA obtained from a WT (*Sirt1*$^{+/+}$ and *SM22a-Cre*$^{-/-}$), a heterozygous (*Sirt1*$^{flox/+}$ and *SM22a-Cre*$^{+/-}$), and a homozygous (*Sirt1*$^{flox/flox}$ and *SM22a-Cre*$^{+/+}$) mouse. (**D**) Western blotting for assessing the expression of Sirt1 in mouse VSMCs obtained from the aortas of control mice (*SM22a-Cre*$^{-/-}$*; Sirt1*$^{flox/flox}$) and VSMC-specific *Sirt1* KO mice (*SM22a-Cre*$^{+/-}$*; Sirt1*$^{flox/flox}$). (**E**) Quantitative analysis of SIRT1 activity in aorta homogenates from WT and SV-KO mice ($n$=6 per group). (**F**) Representative Western blots of SIRT1 in the tissues of WT and SV-KO mice.

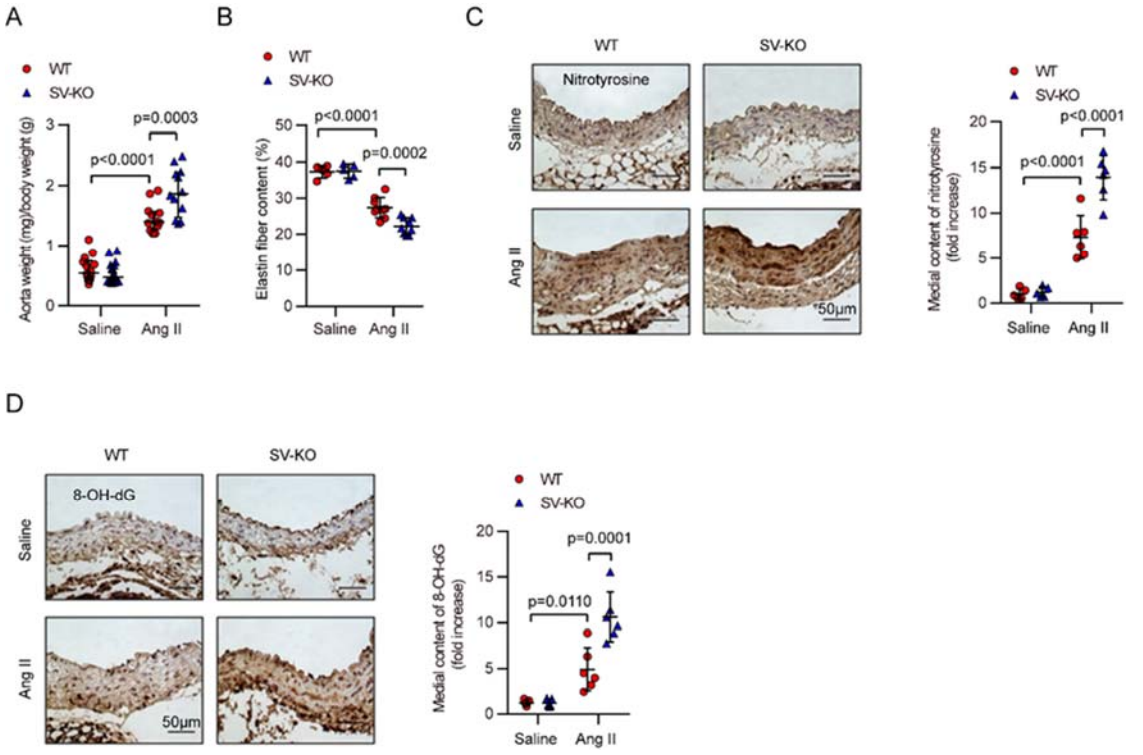


**Online Figure Ⅲ** VSMC-specific SIRT1 ablation promotes AAA formation and ROS production induced by Ang II infusion. (**A**) The ratio of aorta weight to body weight in saline- and Ang II-infused WT or SV-KO mice. **(B)** The elastin fiber content in suprarenal aortas from saline- and Ang II-infused WT or SV-KO mice. **(C)** Representative immunostaining and densitometric analysis of the medial nitrotyrosine in the suprarenal aortic wall of WT and SV-KO mice infused with saline or Ang II for 4 weeks (*n*=5-6 per group). Scale bars, 50 μm. (**D**) Representative immunostaining and densitometric analysis of the medial 8-OH-dG content in the suprarenal aortic wall of WT and SV-KO mice infused with saline or Ang II for 4 weeks (*n*=5-6 per group). Scale bars, 50 μm.

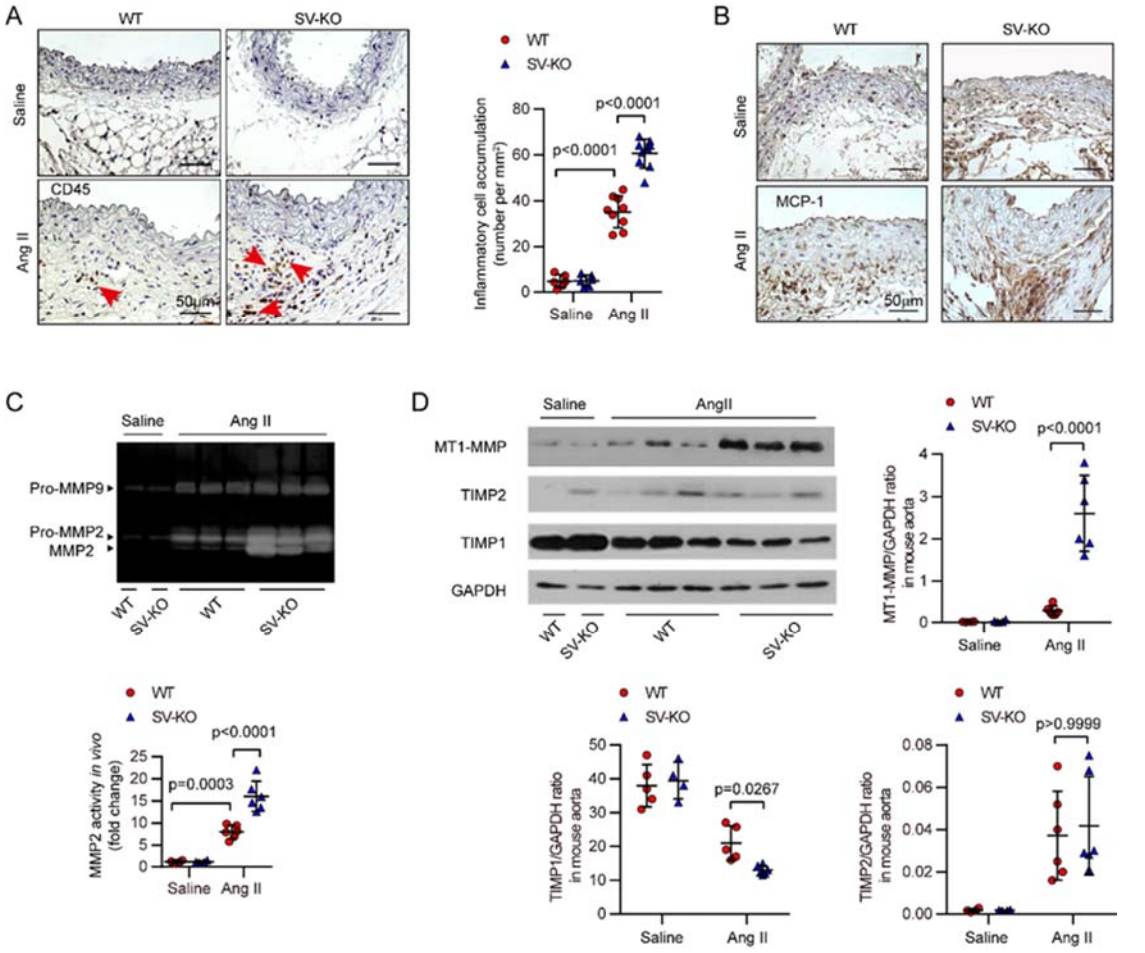


**Online Figure Ⅳ** Increased inflammatory response and MMP activation in the aortas of Ang II-infused SV-KO mice. **(A)** Representative immunostaining and densitometric analysis of CD45 in the suprarenal aortic wall of WT and SV-KO mice infused with saline or Ang II for 4 weeks. The arrows show representative staining with CD45 antibody (n=6-9 per group). Scale bars, 50 μm. (**B**) Representative immunostaining of MCP-1/CCL2 in the suprarenal aortic wall of saline and Ang II-infused mice (scale bars, 50 μm). **(C)** Aorta homogenates were obtained from WT and SV-KO mice infused with saline or Ang II for 4 weeks and MMP activities were examined by zymography. Representative images and densitometric analysis of MMP activities in aorta homogenates (n=4-6 per group). (**D**) Aorta homogenates were obtained from WT and SV-KO mice infused with saline or Ang II for 4 weeks. Western blot and densitometric analysis of protein levels of the MT1-MMP, TIMP1, and TIMP2 in aorta homogenates (n=4-6 per group).

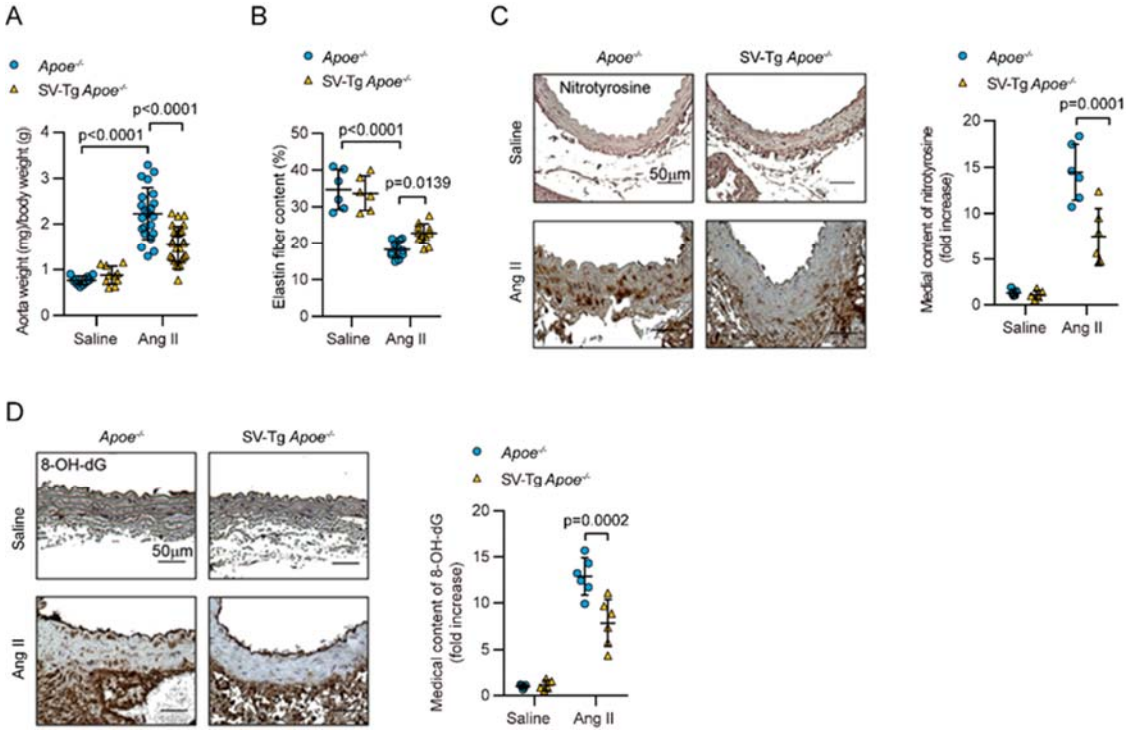


**Online Figure** Ⅴ SIRT1 transgene attenuates AAA formation and ROS production in the aortas of Ang II-infused *Apoe*$^{-/-}$ mice. (**A**) The ratio of aorta weight to body weight in saline- and Ang II-infused *Apoe*$^{-/-}$ or SV-Tg *Apoe*$^{-/-}$ mice. **(B)** The elastin fiber content in suprarenal aortas from saline- and Ang II-infused *Apoe*$^{-/-}$ or SV-Tg *Apoe*$^{-/-}$ mice. **(C)** Representative immunostaining and densitometric analysis of the medial nitrotyrosine in the suprarenal aortic wall of *Apoe*$^{-/-}$ and SV-Tg *Apoe*$^{-/-}$ mice infused with saline or Ang II for 4 weeks (*n*=5-6 per group). Scale bars, 50 μm. (**D**) Representative immunostaining and densitometric analysis of the medial 8-OH-dG content in the suprarenal aortic wall of *Apoe*$^{-/-}$ and SV-Tg *Apoe*$^{-/-}$ mice infused with saline or Ang II for 4 weeks (*n*=5-6 per group). Scale bars, 50 μm.

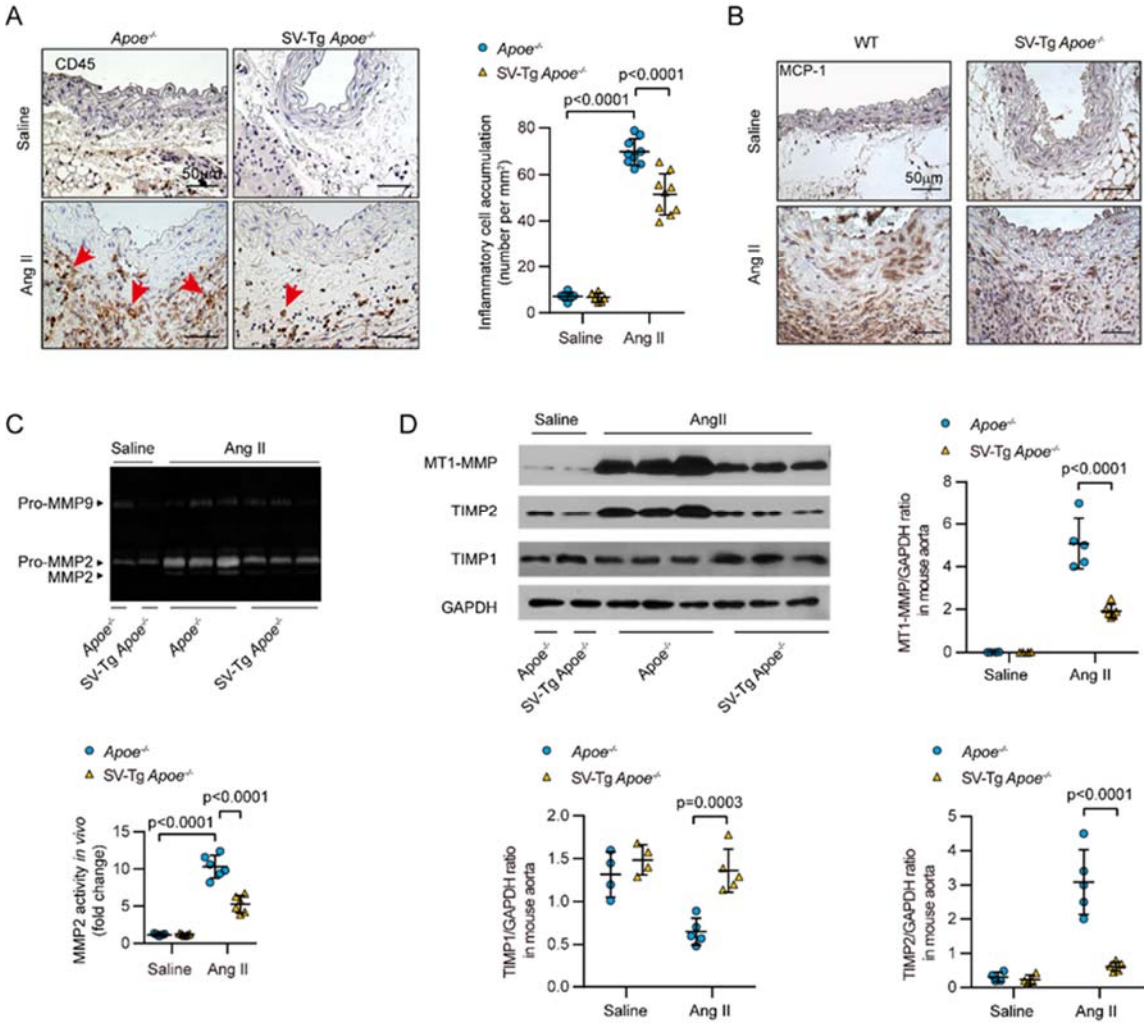


**Online Figure Ⅵ** SIRT1 transgene decreases inflammatory response and MMP activation in the aortas of Ang II-infused *Apoe*$^{-/-}$ mice. **(A)** Representative immunostaining and densitometric analysis of CD45 in the suprarenal aortic wall of *Apoe*$^{-/-}$ and SV-Tg *Apoe*$^{-/-}$ mice infused with saline or Ang II for 4 weeks. The arrows show representative staining with CD45 antibody (n=6-9 per group). Scale bars, 50 μm. (**B**) Representative immunostaining of MCP-1/CCL2 in the suprarenal aortic wall of saline and Ang II-infused mice (scale bars, 50 μm). **(C)** Aorta homogenates were obtained from *Apoe*$^{-/-}$ and SV-Tg *Apoe*$^{-/-}$ mice infused with saline or Ang II for 4 weeks and MMP activities were examined by zymography. Representative images and densitometric analysis of MMP activities in aorta homogenates (n=4-6 per group). (**D**) Aorta homogenates were obtained from *Apoe*$^{-/-}$ and SV-Tg *Apoe*$^{-/-}$ mice infused with saline or Ang II for 4 weeks. Western blot and densitometric analysis of protein levels of the MT1-MMP, TIMP1, and TIMP2 in aorta homogenates (n=4-6 per group).

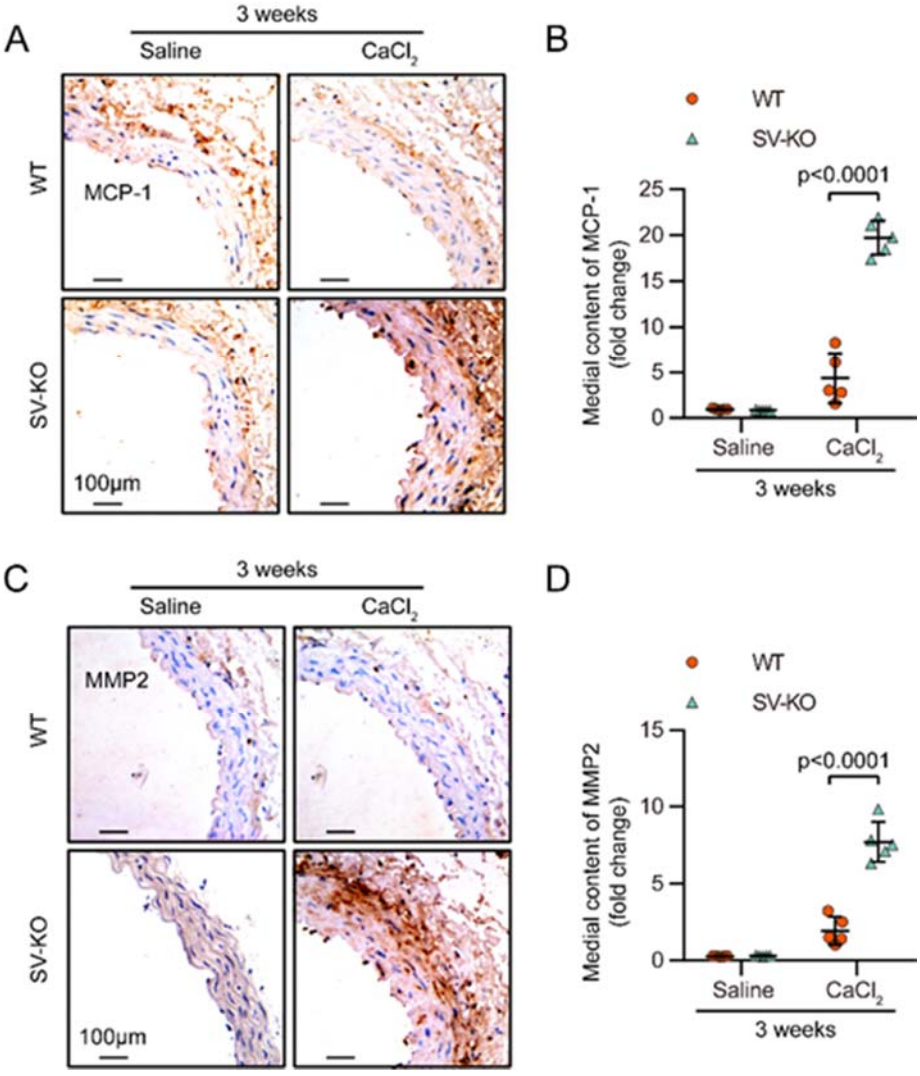


**Online Figure Ⅶ** Increased MCP-1/CCL2 and MT1-MMP expression in the infrarenal aortas of $CaCl_2$-induced SV-KO mice. **(A)** Representative immunostaining of MCP-1/CCL2 in the infrarenal aortic wall of WT and SV-KO mice 3 weeks after treated with saline or $CaCl_2$ (scale bars, 100 μm). (**B**) Densitometric analysis of the medial MCP-1/CCL2 content in the infrarenal aortic wall of WT and SV-KO mice treated with saline or $CaCl_2$ (n=5 per group). (**C**) Representative immunostaining with MMP-2 in the infrarenal aortic wall of WT and SV-KO mice 3 weeks after treated with saline or $CaCl_2$ (scale bars, 100 μm). (**D**) Densitometric analysis of the medial MMP2 content in the infrarenal aortic wall of WT and SV-KO mice treated with saline or $CaCl_2$ (n=5 per group).

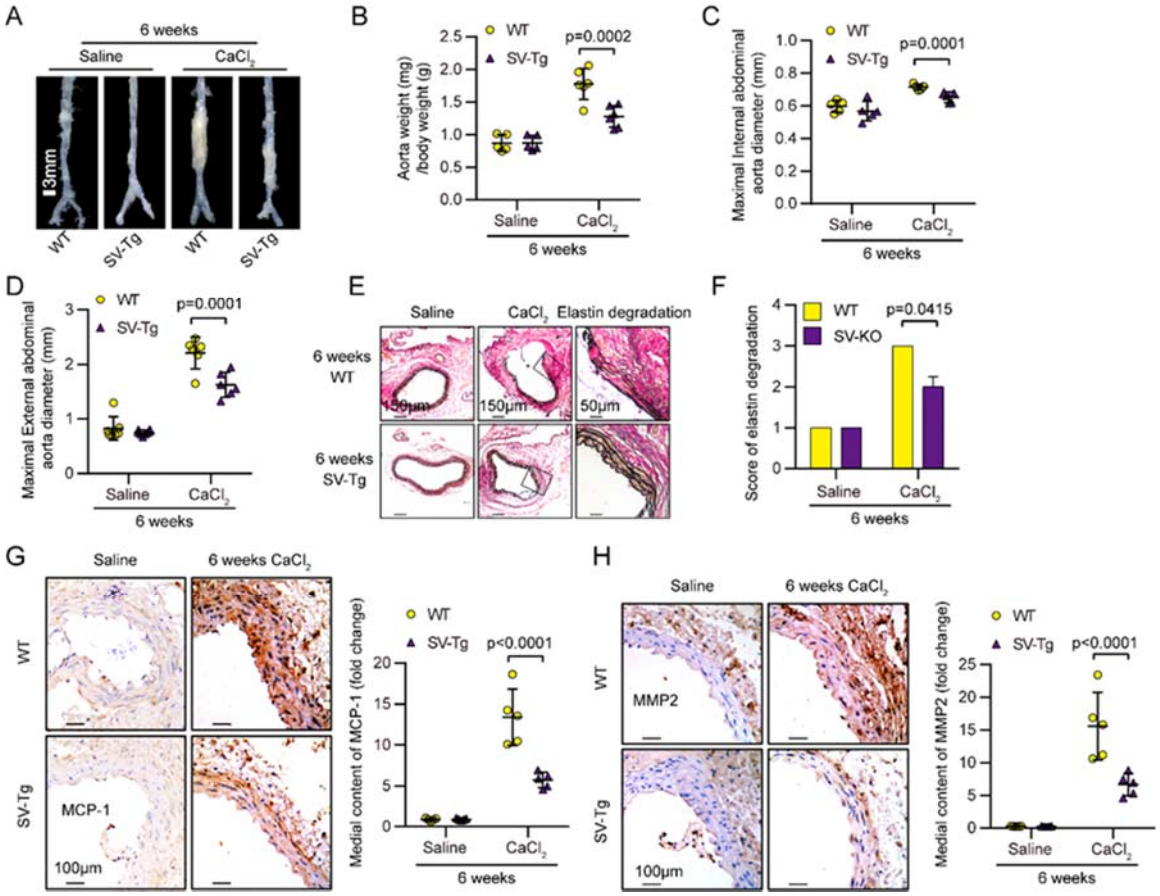


**Online Figure Ⅷ** SIRT1 transgene inhibits $CaCl_2$-induced AAA formation and related vascular pathological changes. **(A)** Representative photographs showing macroscopic features of aneurysms induced by $CaCl_2$ in WT and SV-Tg mice for 6 weeks (scale bars, 3 mm). **(B)** The ratio of aorta weight to body weight in saline- or $CaCl_2$-treated mice. **(C-D)** The maximal internal **(C)** and external diameter **(D)** of infrarenal aortas in WT (n=5-8) and SV-Tg mice (n=5-8) six weeks after treatment with saline or $CaCl_2$. **(E)** Representative staining with elastin in infrarenal aortas from saline- or $CaCl_2$-treated mice (scale bars, 150 μm and 50 μm in magnified photographs). **(F)** Elastin degradation score in infrarenal aortas from saline- or $CaCl_2$-treated mice (n=5-8 per group). (**G**) Representative immunostaining and densitometric analysis of MCP-1/CCL2 in the infrarenal aortic wall of WT and SV-Tg mice 6 weeks after treated with saline or $CaCl_2$ (scale bars, 100 μm) (n=5 per group). (**H**) Representative immunostaining and densitometric analysis of MMP-2 in the infrarenal aortic wall of WT and SV-Tg mice 6 weeks after treated with saline or $CaCl_2$ (scale bars, 100 μm) (n=5 per group).

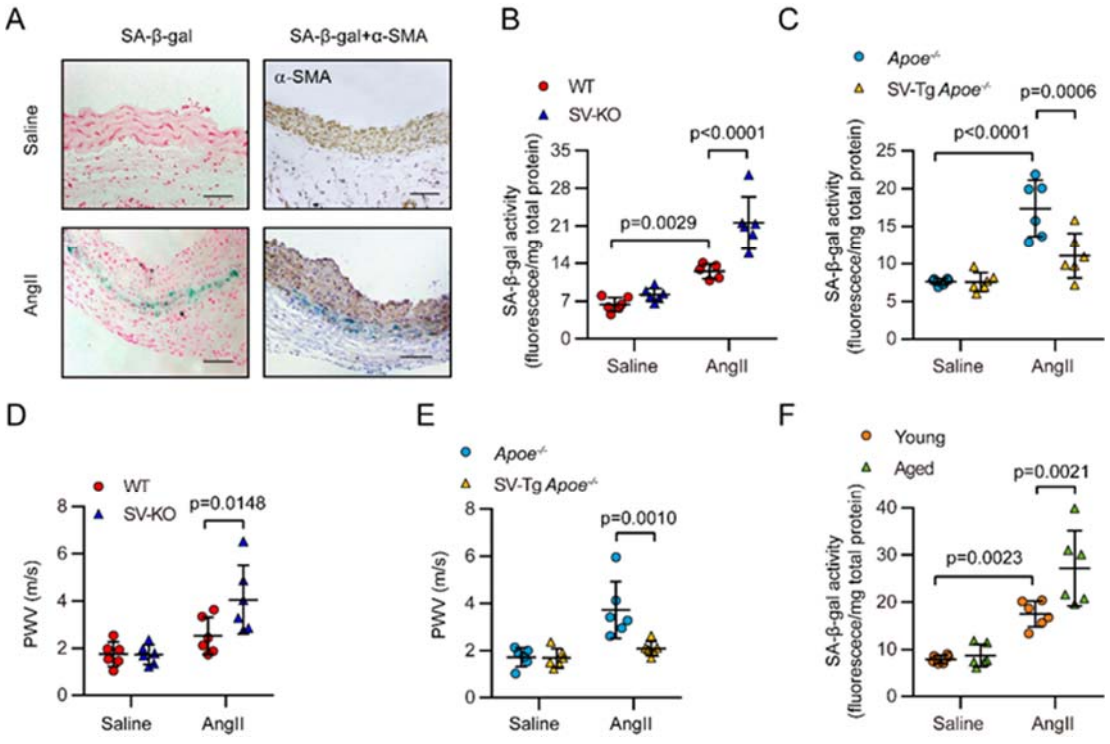


**Online Figure Ⅸ** VSMC-derived SIRT1 is involved in Ang II-induced vascular aging. (**A**) Representative staining of SA-β-gal and α-SMA in the abdominal aorta of saline and Ang II-infused *Apoe*$^{-/-}$ mice. Nuclei were counterstained by Nuclear Fast Red (scale bars, 50 μm). **(B, C, F)** SA-β-gal activity assay results of aorta homogenates from WT and SV-KO **(B)**, *Apoe*$^{-/-}$ and SV-Tg *Apoe*$^{-/-}$ **(C)**, young and aged **(F)** mice infused with saline or Ang II ($n$=5-6 per group). (**D-E**) Quantitative analysis of PWV performed on the LCCA of indicated groups ($n$=6-10 per group).

**A**

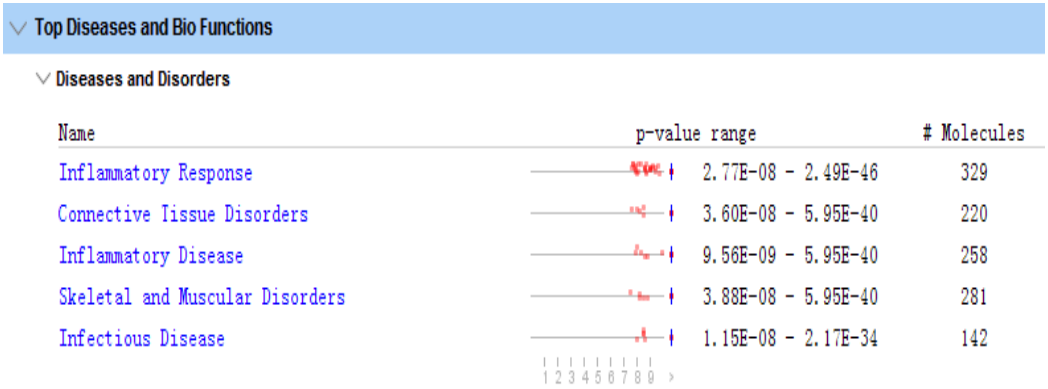
Top Diseases and Bio Functions
Diseases and Disorders
Name
p-value range
# Molecules
Inflammatory Response
2.77E-08 - 2.49E-46
329
Connective Tissue Disorders
3.60E-08 - 5.95E-40
220
Inflammatory Disease
9.56E-09 - 5.95E-40
258
Skeletal and Muscular Disorders
3.88E-08 - 5.95E-40
281
Infectious Disease
1.15E-08 - 2.17E-34
142
1 2 3 4 5 6 7 8 9 ›

**B**

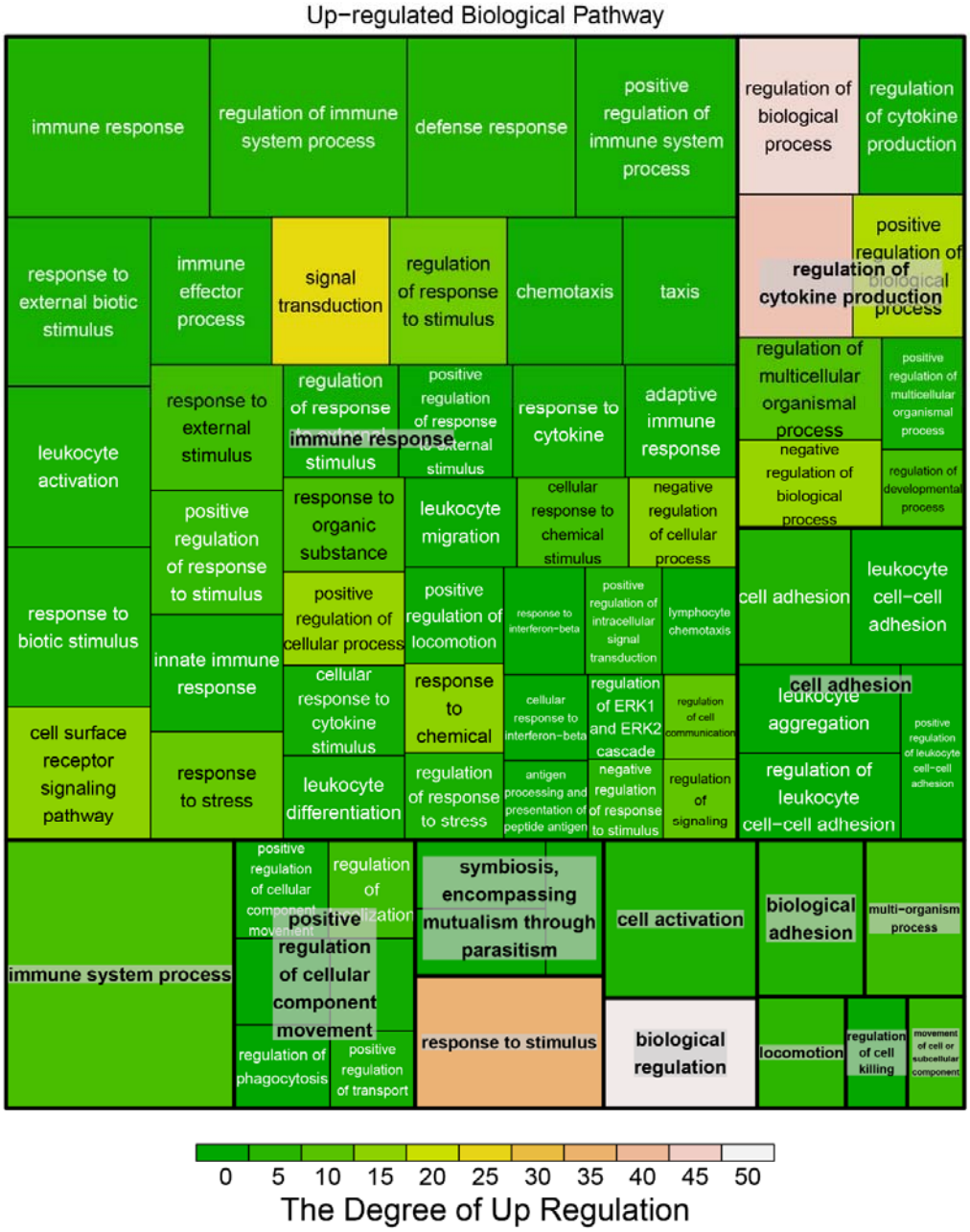


**Online Figure** X Results of IPA analysis. Gene expression microarray analysis was performed using RNA isolated from the aortas of Ang II-treated SV-KO mice and their *Sirt1*$^{flox/flox}$ littermates. Briefly, SV-KO mice and their *Sirt1*$^{flox/flox}$ littermates were subjected to Ang II infusion, and 4 arteries were collected at 4 weeks after Ang II infusion as one sample, and the samples from both SV-KO mice and their *Sirt1*$^{flox/flox}$ littermates were performed for the microarray assay. Microarray data analysis identified 1159 genes that were differentially expressed including 911 upregulated and 248 downregulated genes in the Ang II-treated SV-KO compared with those of Ang II-treated *Sirt1*$^{flox/flox}$ littermates. (**A**) Functional analysis of these genes using Ingenuity Pathway Analysis (IPA) software revealed that

Inflammatory Response was the most affected functions. (**B**) The sub-categories of inflammatory response associated with inflammatory cell recruitment, infiltration and activation are significantly activated in aortas of Ang II-treated SV-KO mice compared with those of Ang II-treated *Sirt1*$^{flox/flox}$ littermates. The color represent the degree of up regulation and the size is determined by the –log10 (p value).

**A**

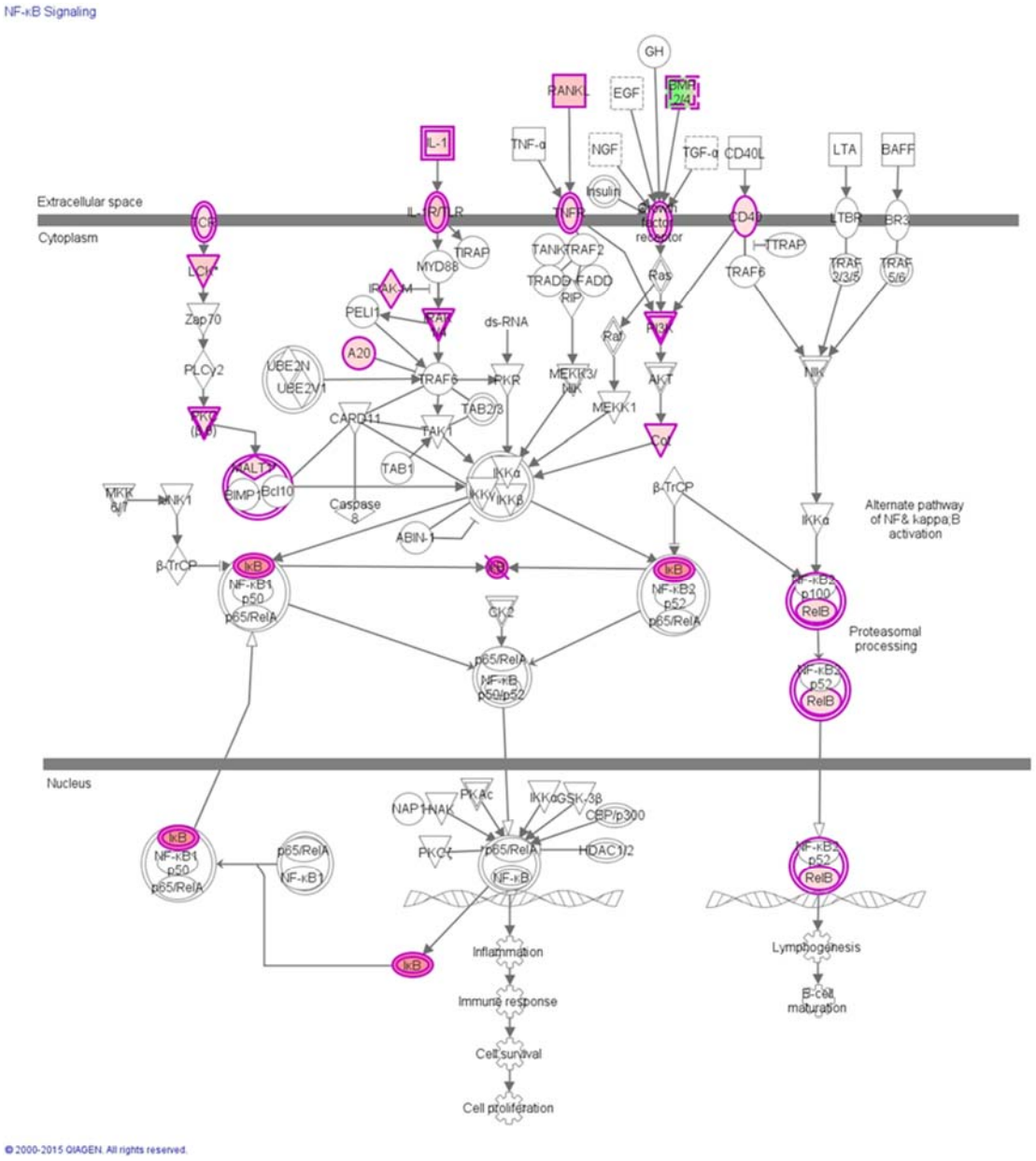

**B**

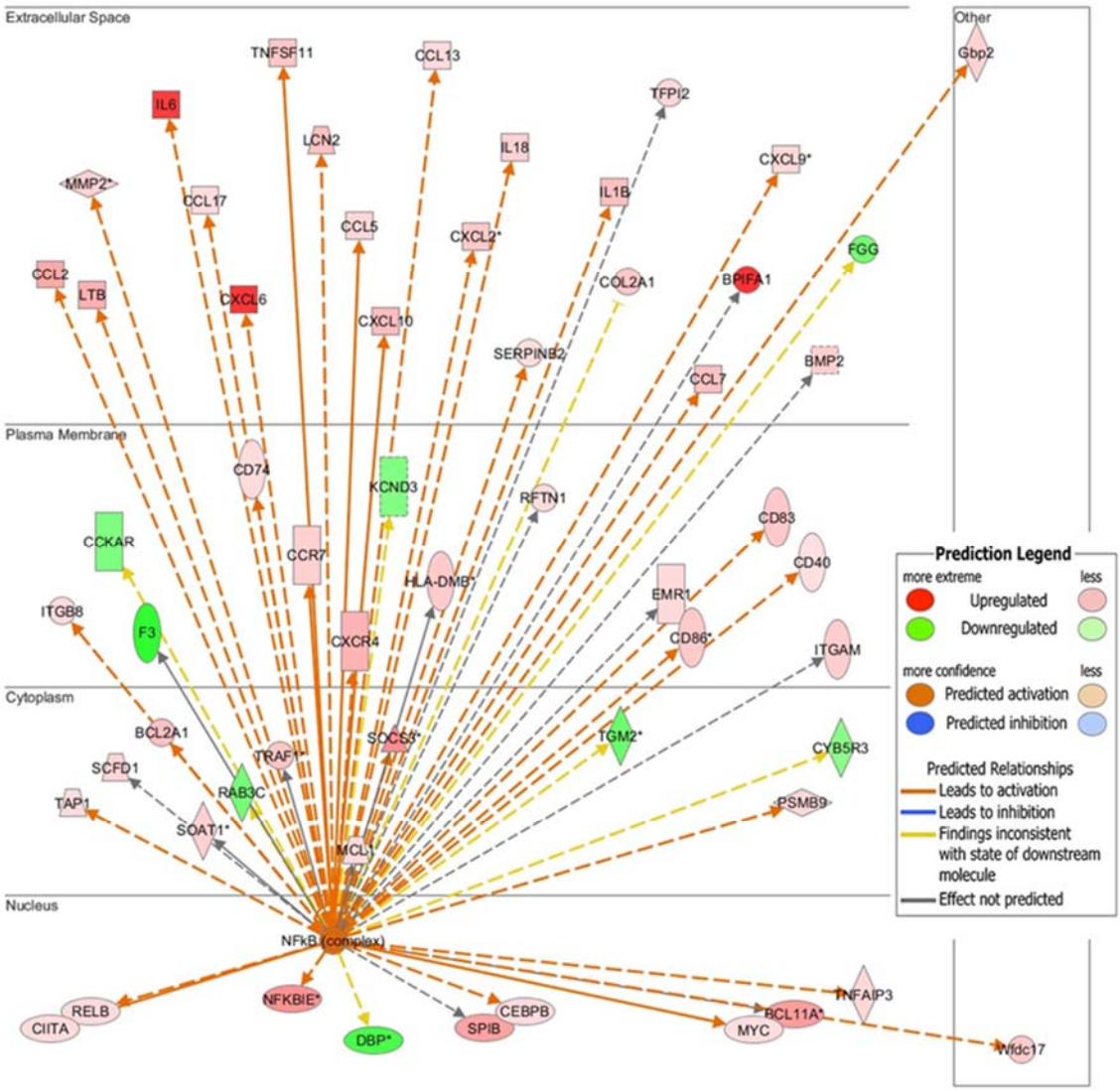
Extracellular Space
Other
Plasma Membrane
Cytoplasm
Nucleus
TNFSF11
CCL13
IL6
LCN2
IL18
TFPI2
CXCL9*
MMP2*
CCL17
CCL5
CXCL2*
IL1B
FGG
CCL2
LTB
CXCL6
CXCL10
COL2A1
BPIFA1
SERPINB2
BMP2
CCL7
CD74
KCND3
RFTN1
CD83
CCKAR
CCR7
HLA-DMB
CD40
ITGB8
F3
CXCR4
EMR1
CD86*
ITGAM
BCL2A1
SOCS3*
TGM2*
CYB5R3
SCFD1
TRAF1*
RAB3C
PSMB9
TAP1
SOAT1*
MCL1*
NFkB (complex)
NFKBIE*
TNFAIP3
RELB
CEBPB
BCL11A*
CIITA
SPIB
MYC
DBP*
Wfdc17
Gbp2
Prediction Legend
more extreme
less
Upregulated
Downregulated
more confidence
Predicted activation
Predicted inhibition
Predicted Relationships
Leads to activation
Leads to inhibition
Findings inconsistent with state of downstream molecule
Effect not predicted

**C**

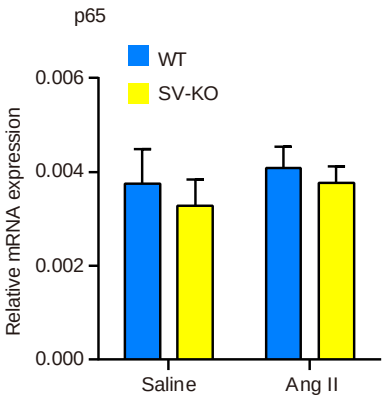
p65
WT
SV-KO
Relative mRNA expression
0.006
0.004
0.002
0.000
Saline
Ang II

**D**

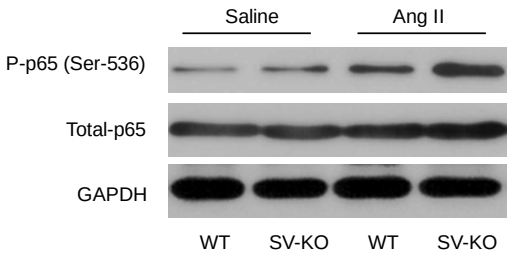
Saline
Ang II
P-p65 (Ser-536)
Total-p65
GAPDH
WT
SV-KO
WT
SV-KO

**Online Figure XI** VSMC-specific SIRT1 ablation activates NF-κB signaling pathway and NF-κB target genes including CCL2/MCP-1 in Ang II-induced AAAs (**A**) Canonical pathway analysis revealed that NF-κB signaling was strongly affected (z-score: 3.657, *P*-value: 4.03E-07) in aortas of Ang II-treated SV-KO mice compared with those of Ang II-treated $Sirt1^{flox/flox}$ littermates. (**B**) IPA upstream regulator analysis showed that NF-κB was significantly activated in aortas of Ang II-treated SV-KO mice compared with those of Ang II-treated $Sirt1^{flox/flox}$ littermates. It was the most important inflammatory transcription regulator (TR) altered. The target genes regulated by NF-κB in aortas of Ang II-treated SV-KO mice including MCP-1, also known as CCL2, a critical chemokine for inflammatory cell recruitment SV-KO mice. (**C**) The mRNA level of p65 in the aortas of SV-KO and WT mice infused with saline or Ang II for 4 weeks. (**D**) Representative Western blot of phosphorylation of p65 and total p65 in aorta homogenates from SV-KO and WT mice infused with saline or Ang II for 4 weeks.

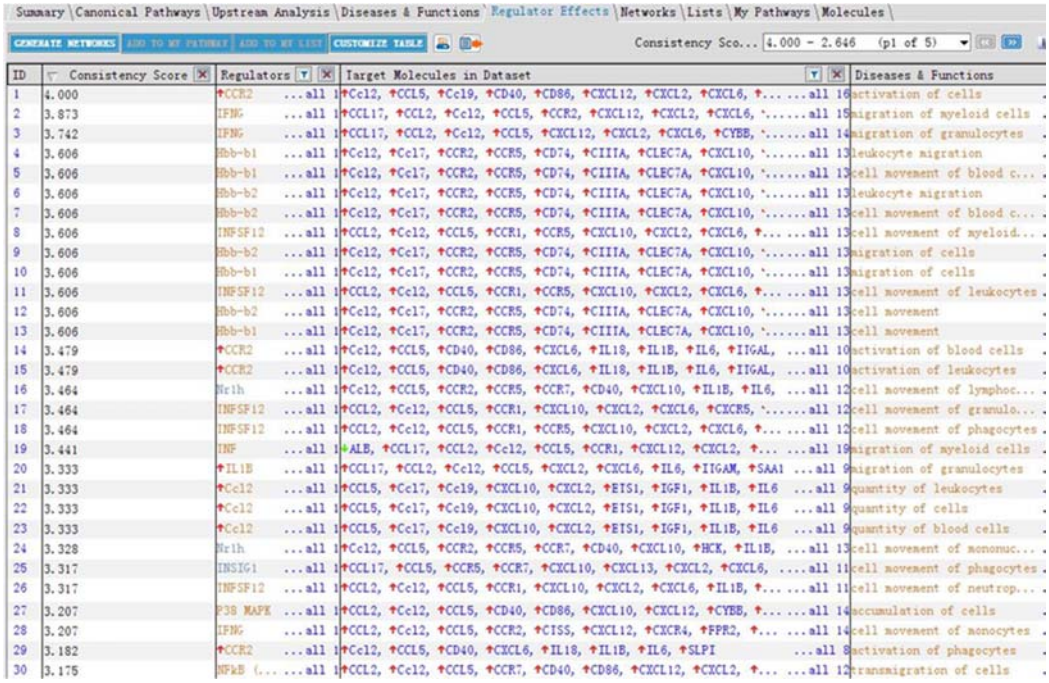

Summary | Canonical Pathways | Upstream Analysis | Diseases & Functions | Regulator Effects | Networks | Lists | My Pathways | Molecules

GENERATE NETWORKS | ADD TO MY PATHWAY | ADD TO MY LIST | CUSTOMIZE TABLE | Consistency Sco... 4.000 - 2.646 (p1 of 5)

| ID | Consistency Score | Regulators | | Target Molecules in Dataset | | Diseases & Functions |
|---|---|---|---|---|---|---|
| 1 | 4.000 | ↑CCR2 | ...all 1 | ↑Ccl2, ↑CCL5, ↑Cc19, ↑CD40, ↑CD86, ↑CXCL12, ↑CXCL2, ↑CXCL6, ↑... | ...all 16 | activation of cells |
| 2 | 3.873 | IFNG | ...all 1 | ↑CCL17, ↑CCL2, ↑Cc12, ↑CCL5, ↑CCR2, ↑CXCL12, ↑CXCL2, ↑CXCL6, ↑..... | ...all 15 | migration of myeloid cells |
| 3 | 3.742 | IFNG | ...all 1 | ↑CCL17, ↑CCL2, ↑Cc12, ↑CCL5, ↑CXCL12, ↑CXCL2, ↑CXCL6, ↑CYBB, ↑..... | ...all 14 | migration of granulocytes |
| 4 | 3.606 | Hbb-b1 | ...all 1 | ↑Cc12, ↑Cc17, ↑CCR2, ↑CCR5, ↑CD74, ↑CIITA, ↑CLEC7A, ↑CXCL10, ↑..... | ...all 13 | leukocyte migration |
| 5 | 3.606 | Hbb-b1 | ...all 1 | ↑Cc12, ↑Cc17, ↑CCR2, ↑CCR5, ↑CD74, ↑CIITA, ↑CLEC7A, ↑CXCL10, ↑..... | ...all 13 | cell movement of blood c... |
| 6 | 3.606 | Hbb-b2 | ...all 1 | ↑Cc12, ↑Cc17, ↑CCR2, ↑CCR5, ↑CD74, ↑CIITA, ↑CLEC7A, ↑CXCL10, ↑..... | ...all 13 | leukocyte migration |
| 7 | 3.606 | Hbb-b2 | ...all 1 | ↑Cc12, ↑Cc17, ↑CCR2, ↑CCR5, ↑CD74, ↑CIITA, ↑CLEC7A, ↑CXCL10, ↑..... | ...all 13 | cell movement of blood c... |
| 8 | 3.606 | INFSF12 | ...all 1 | ↑CCL2, ↑Cc12, ↑CCL5, ↑CCR1, ↑CCR5, ↑CXCL10, ↑CXCL2, ↑CXCL6, ↑... | ...all 13 | cell movement of myeloid... |
| 9 | 3.606 | Hbb-b2 | ...all 1 | ↑Cc12, ↑Cc17, ↑CCR2, ↑CCR5, ↑CD74, ↑CIITA, ↑CLEC7A, ↑CXCL10, ↑..... | ...all 13 | migration of cells |
| 10 | 3.606 | Hbb-b1 | ...all 1 | ↑Cc12, ↑Cc17, ↑CCR2, ↑CCR5, ↑CD74, ↑CIITA, ↑CLEC7A, ↑CXCL10, ↑..... | ...all 13 | migration of cells |
| 11 | 3.606 | INFSF12 | ...all 1 | ↑CCL2, ↑Cc12, ↑CCL5, ↑CCR1, ↑CCR5, ↑CXCL10, ↑CXCL2, ↑CXCL6, ↑... | ...all 13 | cell movement of leukocytes |
| 12 | 3.606 | Hbb-b2 | ...all 1 | ↑Cc12, ↑Cc17, ↑CCR2, ↑CCR5, ↑CD74, ↑CIITA, ↑CLEC7A, ↑CXCL10, ↑..... | ...all 13 | cell movement |
| 13 | 3.606 | Hbb-b1 | ...all 1 | ↑Cc12, ↑Cc17, ↑CCR2, ↑CCR5, ↑CD74, ↑CIITA, ↑CLEC7A, ↑CXCL10, ↑..... | ...all 13 | cell movement |
| 14 | 3.479 | ↑CCR2 | ...all 1 | ↑Cc12, ↑CCL5, ↑CD40, ↑CD86, ↑CXCL6, ↑IL18, ↑IL1B, ↑IL6, ↑IIGAL, | ...all 10 | activation of blood cells |
| 15 | 3.479 | ↑CCR2 | ...all 1 | ↑Cc12, ↑CCL5, ↑CD40, ↑CD86, ↑CXCL6, ↑IL18, ↑IL1B, ↑IL6, ↑IIGAL, | ...all 10 | activation of leukocytes |
| 16 | 3.464 | Nr1h | ...all 1 | ↑Cc12, ↑CCL5, ↑CCR2, ↑CCR5, ↑CCR7, ↑CD40, ↑CXCL10, ↑IL1B, ↑IL6, | ...all 12 | cell movement of lymphoc... |
| 17 | 3.464 | INFSF12 | ...all 1 | ↑CCL2, ↑Cc12, ↑CCL5, ↑CCR1, ↑CXCL10, ↑CXCL2, ↑CXCL6, ↑CXCR5, ↑..... | ...all 12 | cell movement of granulo... |
| 18 | 3.464 | INFSF12 | ...all 1 | ↑CCL2, ↑Cc12, ↑CCL5, ↑CCR1, ↑CCR5, ↑CXCL10, ↑CXCL2, ↑CXCL6, ↑... | ...all 12 | cell movement of phagocytes |
| 19 | 3.441 | INF | ...all 1 | ↓ALB, ↑CCL17, ↑CCL2, ↑Cc12, ↑CCL5, ↑CCR1, ↑CXCL12, ↑CXCL2, ↑... | ...all 19 | migration of myeloid cells |
| 20 | 3.333 | ↑IL1B | ...all 1 | ↑CCL17, ↑CCL2, ↑Cc12, ↑CCL5, ↑CXCL2, ↑CXCL6, ↑IL6, ↑IIGAM, ↑SAA1 | ...all 9 | migration of granulocytes |
| 21 | 3.333 | ↑Ccl2 | ...all 1 | ↑CCL5, ↑Cc17, ↑Cc19, ↑CXCL10, ↑CXCL2, ↑EIS1, ↑IGF1, ↑IL1B, ↑IL6 | ...all 9 | quantity of leukocytes |
| 22 | 3.333 | ↑Ccl2 | ...all 1 | ↑CCL5, ↑Cc17, ↑Cc19, ↑CXCL10, ↑CXCL2, ↑EIS1, ↑IGF1, ↑IL1B, ↑IL6 | ...all 9 | quantity of cells |
| 23 | 3.333 | ↑Ccl2 | ...all 1 | ↑CCL5, ↑Cc17, ↑Cc19, ↑CXCL10, ↑CXCL2, ↑EIS1, ↑IGF1, ↑IL1B, ↑IL6 | ...all 9 | quantity of blood cells |
| 24 | 3.328 | Nr1h | ...all 1 | ↑Cc12, ↑CCL5, ↑CCR2, ↑CCR5, ↑CCR7, ↑CD40, ↑CXCL10, ↑HCK, ↑IL1B, | ...all 13 | cell movement of mononuc... |
| 25 | 3.317 | INSIG1 | ...all 1 | ↑CCL17, ↑CCL5, ↑CCR5, ↑CCR7, ↑CXCL10, ↑CXCL13, ↑CXCL2, ↑CXCL6, | ...all 11 | cell movement of phagocytes |
| 26 | 3.317 | INFSF12 | ...all 1 | ↑CCL2, ↑Cc12, ↑CCL5, ↑CCR1, ↑CXCL10, ↑CXCL2, ↑CXCL6, ↑IL1B, ↑... | ...all 11 | cell movement of neutrop... |
| 27 | 3.207 | P38 MAPK | ...all 1 | ↑CCL2, ↑Cc12, ↑CCL5, ↑CD40, ↑CD86, ↑CXCL10, ↑CXCL12, ↑CYBB, ↑... | ...all 14 | accumulation of cells |
| 28 | 3.207 | IFNG | ...all 1 | ↑CCL2, ↑Cc12, ↑CCL5, ↑CCR2, ↑CISS, ↑CXCL12, ↑CXCR4, ↑FPR2, ↑... | ...all 14 | cell movement of monocytes |
| 29 | 3.182 | ↑CCR2 | ...all 1 | ↑Cc12, ↑CCL5, ↑CD40, ↑CXCL6, ↑IL18, ↑IL1B, ↑IL6, ↑SLPI | ...all 8 | activation of phagocytes |
| 30 | 3.175 | NFkB (... | ...all 1 | ↑CCL2, ↑Cc12, ↑CCL5, ↑CCR7, ↑CD40, ↑CD86, ↑CXCL12, ↑CXCL2, ↑... | ...all 12 | transmigration of cells |

**Online Figure Ⅻ** Most related Regulator Effects in IPA analysis. The Regulator Effects feature in IPA empowers to generate a hypothesis for how a phenotype, function or disease is regulated in the dataset by activated or inhibited upstream regulators. Regulator Effects in IPA analysis showed that the consistency Score of CCR2, the receptor of MCP-1/CCL2 was highest in all the regulators. NF-κB and MCP-1/CCL2 also showed high Consistency Scores for inflammatory cell recruitment, infiltration and activation.

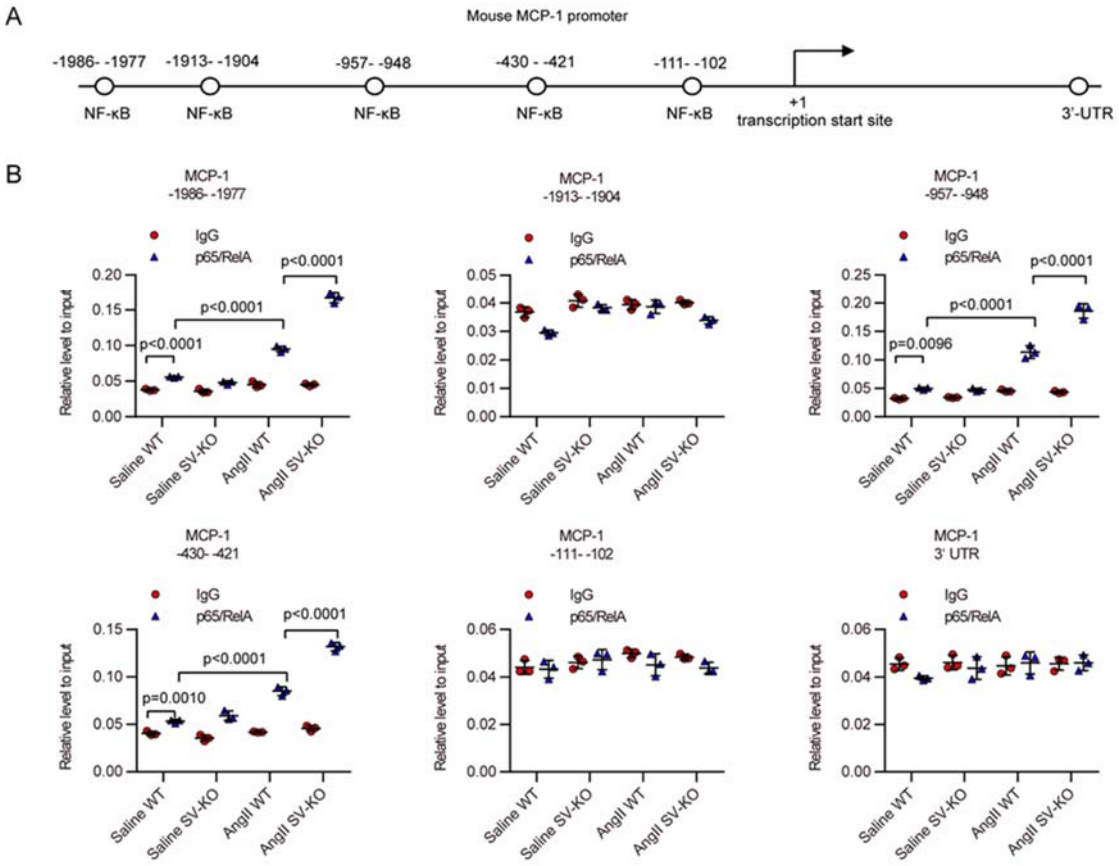


**Online Figure XIII** Loss-of-function of SIRT1 in VSMCs increases NF-κB binding on MCP-1 promoter. Chromatin immunoprecipitation (ChIP) assays were performed with chromatin prepared from aortas of saline and Ang II-infused WT and SV-KO mice. Chromatin was immunoprecipitated with normal rabbit IgG or antibody against p65/RelA, and precipitated genomic DNA was analyzed by real-time polymerase chain reaction using different primers for the indicated areas of the MCP-1 promoters or 3′ -UTR region. (**A**) Diagrammatic drawing shows that the putative binding sites on mouse MCP-1 promoters predicted by software. (**B**) ChIP-qPCR results of binding levels of IgG and p65/RelA on MCP-1 promoter and 3'-UTR. (*n*=3 per group)

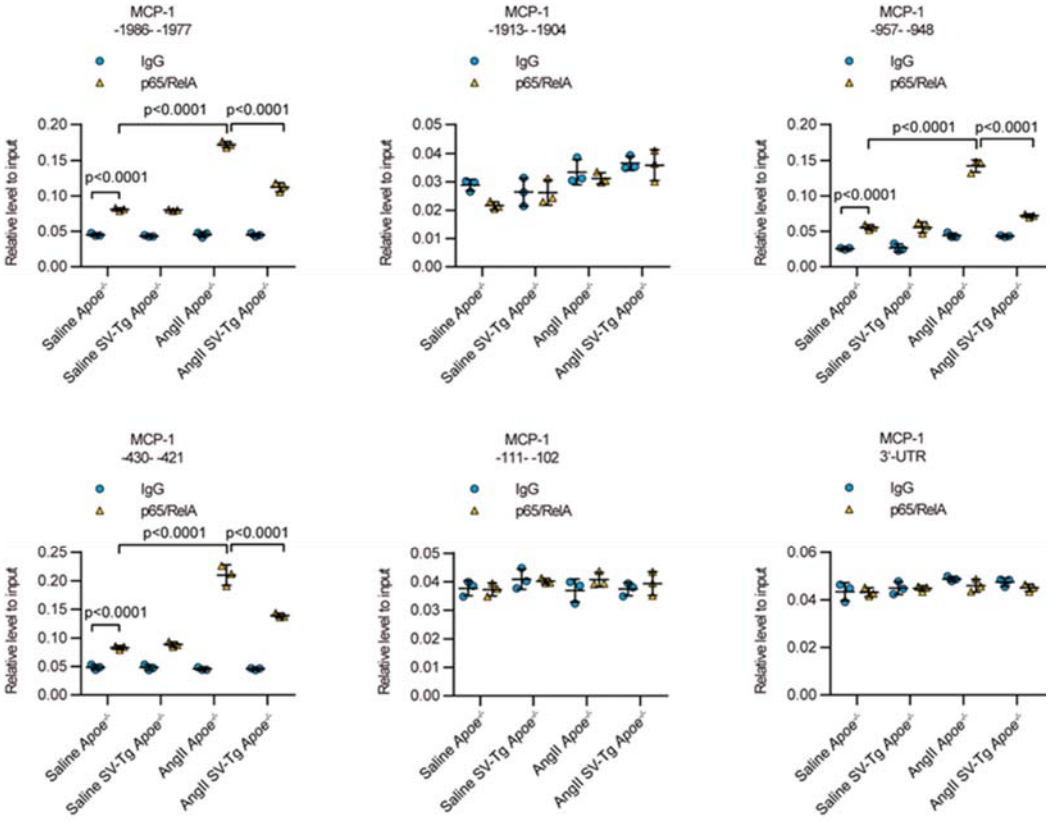


**Online Figure XIV** SIRT1 overexpression inhibits Ang II-increased NF-κB binding on MCP-1 promoter. Chromatin immunoprecipitation (ChIP) assays were performed with chromatin prepared from aortas of saline and Ang II-infused *Apoe*$^{-/-}$ and SV-Tg *Apoe*$^{-/-}$ mice. Chromatin was immunoprecipitated with normal rabbit IgG or antibody against p65/RelA, and precipitated genomic DNA was analyzed by real-time polymerase chain reaction using different primers for the indicated areas of the MCP-1 promoters or 3′ -UTR region. ChIP-qPCR results of binding levels of IgG and p65/RelA on MCP-1 promoter are showed. (n=3 per group)

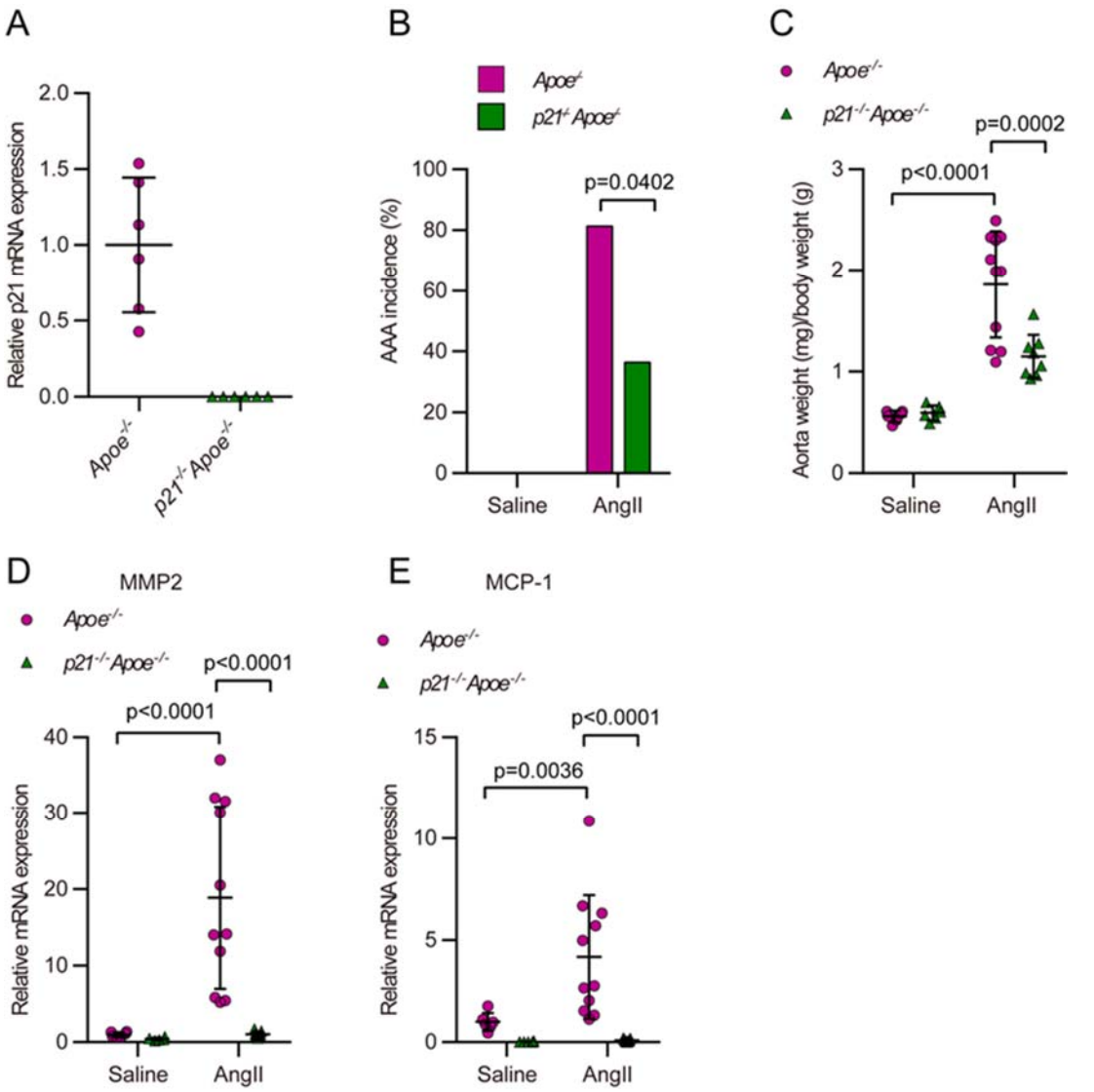


**Online Figure XV** p21 knockout blocks AngII-induced AAAs and expression of MMP-2 and MCP-1 in *Apoe*$^{-/-}$ mice. (**A**) Relative mRNA level of p21 in *Apoe*$^{-/-}$ and *p21*$^{-/-}$*Apoe*$^{-/-}$ mice (n=6). (**B**) The incidence of AngII-induced AAA in *p21*$^{-/-}$*Apoe*$^{-/-}$ mice (*n*=11) compared with that in *Apoe*$^{-/-}$ mice (*n*=16). There was no AAA formation in saline-infused mice (*n*=6 per group), and all deaths were due to aortic rupture. (**C**) The ratio of aorta weight to body weight in saline- and AngII-infused mice. (**D-E**) mRNA levels of MMP-2 (D) and MCP-1 (E) detected by real-time PCR in aorta homogenates from *Apoe*$^{-/-}$ and *p21*$^{-/-}$*Apoe*$^{-/-}$ mice infused with Ang II (*n*=11 for *Apoe*$^{-/-}$; *n*=9 for *p21*$^{-/-}$*Apoe*$^{-/-}$ group) or saline (*n*=6 per group).

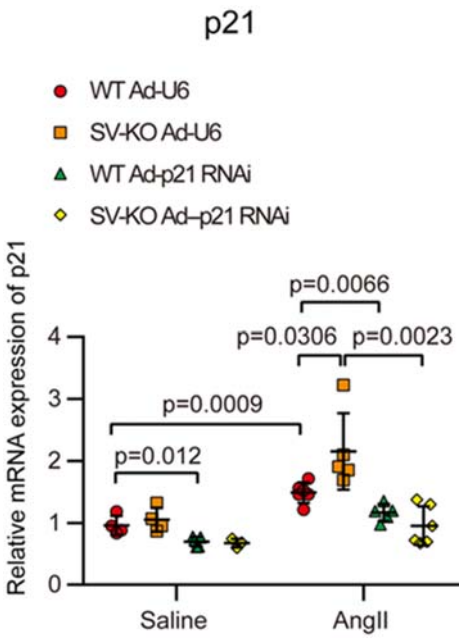


**Online Figure XVI** p21 mRNA level in both saline and Ang II-treated VSMCs was significantly repressed by transfection of Ad-p21 RNAi. Relative p21 mRNA expression level detected by real-time PCR in saline or Ang II-treated WT and SV-KO VSMCs infected with Ad-U6 or Ad-p21 RNAi (n=3-6 per group).

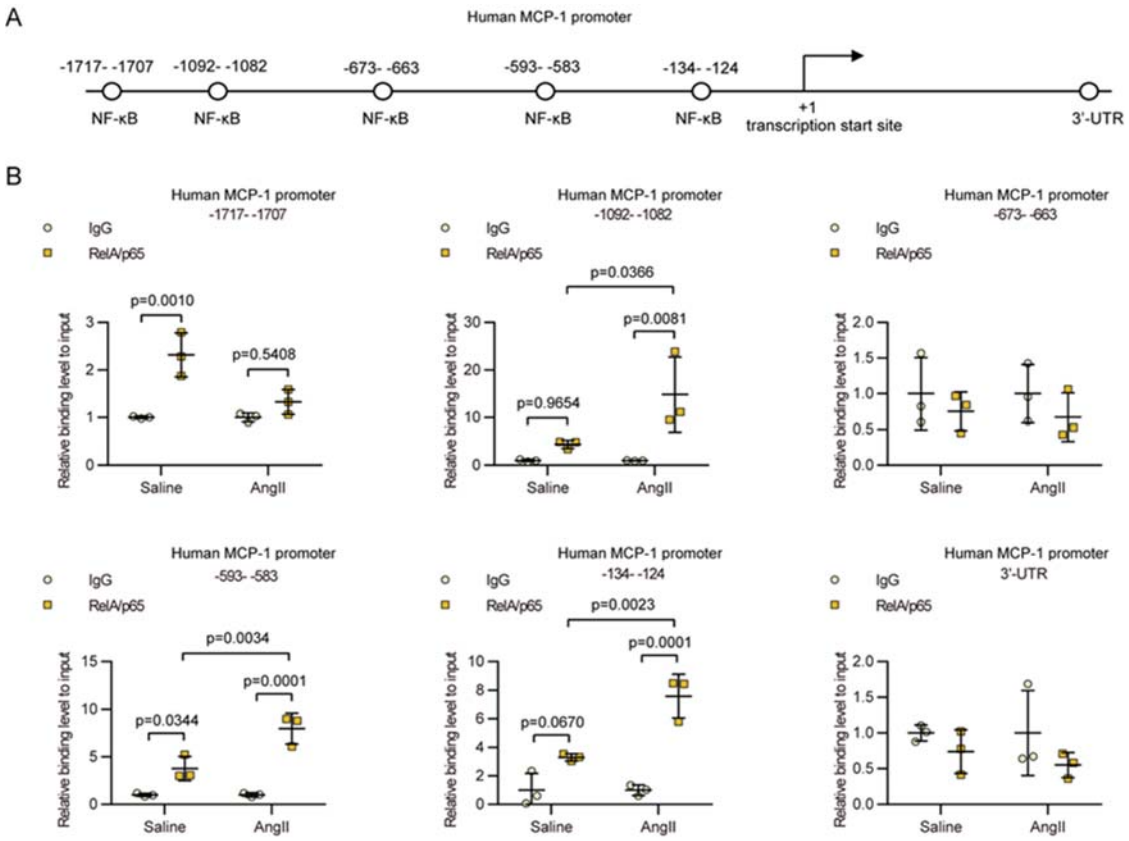


**Online Figure XVII** Ang II treatment increases NF-κB binding on human MCP-1 promoter. Chromatin immunoprecipitation (ChIP) assays were performed with chromatin prepared from saline or Ang II-treated human VSMCs. Chromatin was immunoprecipitated with normal rabbit IgG or antibody against RelA/p65, and precipitated genomic DNA was analyzed by real-time polymerase chain reaction using different primers for the indicated areas of the MCP-1 promoters or 3′ -UTR region. Three binding sites of NF-κB (−1092 to −1082; −593 to −583; −134 to −124) on human MCP-1/CCL2 promoter by ChIP assays were selected out from the 5 potential binding sites to assess the impact of p21 knockdown on the effect of SIRT1 RNAi on transcriptional activation of MCP-1/CCL2. (**A**) Diagrammatic drawing shows that the putative binding sites of NF-κB on human MCP-1 promoters predicted by software. (**B**) ChIP-qPCR results of binding levels of IgG, RelA/p65 on MCP-1 promoter are showed. (*n*=3 per group)

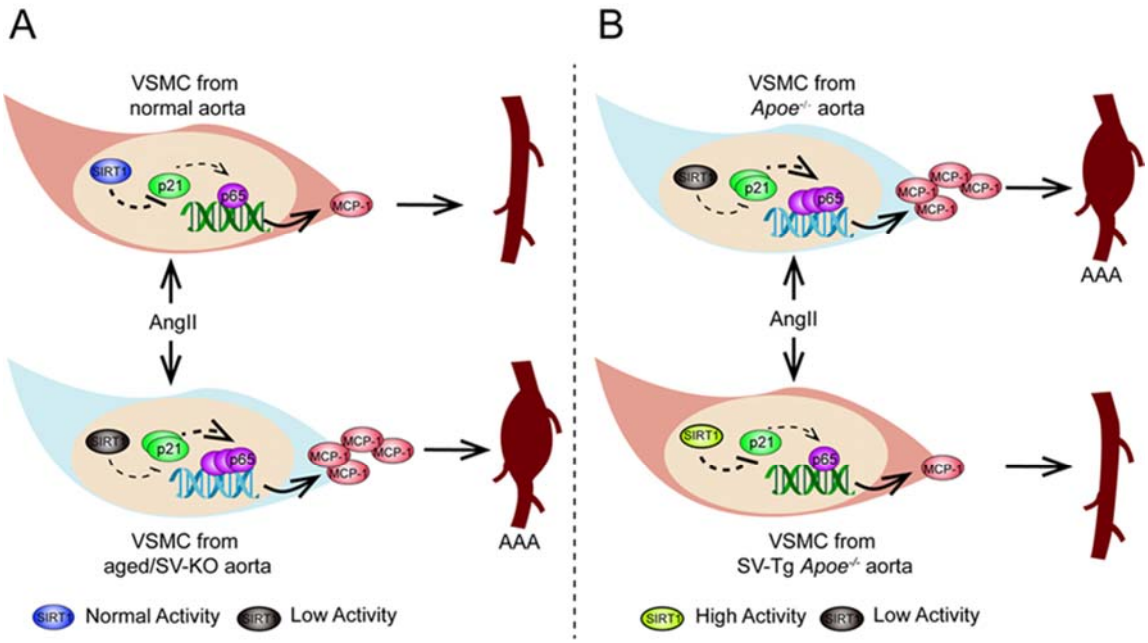


**Online Figure XVIII** Schematic summary. Our results show a direct link between vascular cell senescence and vascular inflammation to AAA formation by SIRT1 reduction and that effective SIRT1 activation in VSMCs might prevent AAA formation. (**A**) SIRT1 expression/activity is decreased in the medial VSMCs of the suprarenal aortas of aged mice. The reduction of SIRT1 increases vascular cell senescence and upregulates the expression of p21 in response to AngII infusion. Accordingly, NF-κB binding activity and MCP-1 expression are increased in VSMCs, which promotes inflammatory cell recruitment to the media, magnifies vascular inflammation and instigates AAA formation. (**B**) VSMC-specific overexpression of SIRT1 can effectively inhibit AAA formation and related pathological and molecular changes.

**References**

1. Li L, Zhang HN, Chen HZ, Gao P, Zhu LH, Li HL, Lv X, Zhang QJ, Zhang R, Wang Z, She ZG, Wei YS, Du GH, Liu DP and Liang CC. SIRT1 acts as a modulator of neointima formation following vascular injury in mice. *Circ Res*. 2011;108:1180-9.
2. Deng C, Zhang P, Harper JW, Elledge SJ and Leder P. Mice lacking p21CIP1/WAF1 undergo normal development, but are defective in G1 checkpoint control. *Cell*. 1995;82:675-84.
3. Satoh K, Nigro P, Matoba T, O'Dell MR, Cui Z, Shi X, Mohan A, Yan C, Abe J, Illig KA and Berk BC. Cyclophilin A enhances vascular oxidative stress and the development of angiotensin II-induced aortic aneurysms. *Nature medicine*. 2009;15:649-56.
4. Longo GM, Xiong W, Greiner TC, Zhao Y, Fiotti N and Baxter BT. Matrix metalloproteinases 2 and 9 work in concert to produce aortic aneurysms. *The Journal of clinical investigation*. 2002;110:625-32.
5. Williams R, Needles A, Cherin E, Zhou YQ, Henkelman RM, Adamson SL and Foster FS. Noninvasive ultrasonic measurement of regional and local pulse-wave velocity in mice. *Ultrasound Med Biol*. 2007;33:1368-75.
6. Gary RK and Kindell SM. Quantitative assay of senescence-associated beta-galactosidase activity in mammalian cell extracts. *Analytical biochemistry*. 2005;343:329-34.
7. Dimri GP, Lee X, Basile G, Acosta M, Scott G, Roskelley C, Medrano EE, Linskens M, Rubelj I, Pereira-Smith O and et al. A biomarker that identifies senescent human cells in culture and in aging skin in vivo. *Proceedings of the National Academy of Sciences of the United States of America*. 1995;92:9363-7.
8. Wan YZ, Gao P, Zhou S, Zhang ZQ, Hao DL, Lian LS, Li YJ, Chen HZ and Liu DP. SIRT1-mediated epigenetic downregulation of plasminogen activator inhibitor-1 prevents vascular endothelial replicative senescence. *Aging cell*. 2014;13:890-9.
9. Ishida T, Ishida M, Suero J, Takahashi M and Berk BC. Agonist-stimulated cytoskeletal reorganization and signal transduction at focal adhesions in vascular smooth muscle cells require c-Src. *J Clin Invest*. 1999;103:789-97.
10. Picard F, Kurtev M, Chung N, Topark-Ngarm A, Senawong T, Machado De Oliveira R, Leid M, McBurney MW and Guarente L. Sirt1 promotes fat mobilization in white adipocytes by repressing PPAR-gamma. *Nature*. 2004;429:771-6.
11. Takemura A, Iijima K, Ota H, Son BK, Ito Y, Ogawa S, Eto M, Akishita M and Ouchi Y. Sirtuin 1 retards hyperphosphatemia-induced calcification of vascular smooth muscle cells. *Arterioscler Thromb Vasc Biol*. 2011;31:2054-62.
12. Zhou S, Chen HZ, Wan YZ, Zhang QJ, Wei YS, Huang S, Liu JJ, Lu YB, Zhang ZQ, Yang RF, Zhang R, Cai H, Liu DP and Liang CC. Repression of P66Shc expression by SIRT1 contributes to the prevention of hyperglycemia-induced endothelial dysfunction. *Circulation research*. 2011;109:639-48.
13. Hawkes SP, Li H and Taniguchi GT. Zymography and reverse zymography for detecting MMPs and TIMPs. *Methods Mol Biol*. 2010;622:257-69.
14. Gao P, Xu TT, Lu J, Li L, Xu J, Hao DL, Chen HZ and Liu DP. Overexpression of SIRT1 in vascular smooth muscle cells attenuates angiotensin II-induced vascular remodeling and hypertension in mice. *Journal of molecular medicine (Berlin, Germany)*. 2014;92:347-57.